Overview: Fusion of Radar Polarimetry and Numerical Atmospheric Modelling Towards an Improved Understanding of Cloud and Precipitation Processes

Silke Trömel[1,2], Clemens Simmer[1], Ulrich Blahak[3], Armin Blanke[1], Florian Ewald[4], Michael Frech[5], Mathias Gergely[5], Martin Hagen[4], Sabine Hörnig[6], Tijana Janjic[7], Heike Kalesse-Los[6], Stefan Kneifel[8], Christoph Knote[7,9], Jana Mendrok[3], Manuel Moser[10,4], Gregor Köcher[7], Kai Mühlbauer[1], Alexander Myagkov[11], Velibor Pejcic[1], Patric Seifert[12], Prabhakar Shrestha[1], Audrey Teisseire[12], Leonie von Terzi[8], Eleni Tetoni[4], Teresa Vogl[6], Christiane Voigt[10,4], Yuefei Zeng[7], Tobias Zinner[7], Johannes Quaas[6]

[1]Institute for Geosciences, Department of Meteorology, University of Bonn, Bonn, 53121, Germany
[2]Laboratory for Clouds and Precipitation Exploration, Geoverbund ABC/J, Bonn, 53121, Germany
[3]Deutscher Wetterdienst (DWD), Offenbach, 63067, Germany
[4]Institute for Physics of the Atmosphere, DLR, Oberpfaffenhofen, 82234, Germany
[5]Deutscher Wetterdienst (DWD), Observatorium Hohenpeißenberg, Hohenpeißenberg, 82383, Germany
[6]Institute for Meteorology, Universität Leipzig, Leipzig, 04103, Germany
[7]Meteorological Institute Munich, Ludwig-Maximilians-Universität München, 80333, Germany
[8]Institute of Geophysics and Meteorology, University of Cologne, 50969, Germany
[9]Faculty of Medicine, University of Augsburg, Augsburg, 86159 Germany
[10]Institute for Physics of the Atmosphere, University Mainz, Mainz, 55099, Germany
[11]Radiometer Physics GmbH, Meckenheim, 53340, Germany
[12]Leibniz Institute for Tropospheric Research (TROPOS), 04318 Leipzig, Germany

Correspondence to: Silke Trömel (silke.troemel@uni-bonn.de)

Abstract. Cloud and precipitation processes are still a main source of uncertainties in numerical weather prediction and climate change projections. The Priority Program "Polarimetric Radar Observations meet Atmospheric Modelling (PROM)", funded by the German Research Foundation (Deutsche Forschungsgemeinschaft, DFG), is guided by the hypothesis that many uncertainties relate to the lack of observations suitable to challenge the representation of cloud and precipitation processes in atmospheric models. Such observations can, however, ~~nowadays~~ at present be provided e.g. by the recently installed dual-polarization C-band weather radar network of the German national meteorological service in synergy with cloud radars and other instruments at German supersites and similar national networks increasingly available worldwide. While polarimetric radars potentially provide valuable in-cloud information e.g. on hydrometeor type, quantity, and microphysical cloud and precipitation processes, and atmospheric models employ increasingly complex microphysical modules, considerable knowledge gaps still exist in the interpretation of the observations and in the optimal microphysics model process formulations.

34 PROM is a coordinated interdisciplinary effort to ~~intensify~~ increase the use of polarimetric radar observations in data
35 assimilation, which requires a thorough evaluation and improvement of parameterizations of moist processes in atmospheric
36 models. As an overview article of the inter-journal special issue "Fusion of radar polarimetry and numerical atmospheric
37 modelling towards an improved understanding of cloud and precipitation processes", this article outlines the knowledge
38 achieved in PROM during the past two years and gives perspectives for the next four years.

1 Introduction and Objectives of the priority program

40 ~~A~~ Among the main sources of uncertainty in the models used in numerical weather prediction (NWP) and climate change
41 projections are the parameterizations of cloud and precipitation processes (Bauer et al., 2015). A major part of these
42 uncertainties can be attributed to missing observations suitable to challenge the representation of cloud and precipitation
43 processes employed in atmospheric models. A wealth of new information on precipitation microphysics and generating
44 processes can be gained from observations from polarimetric weather radars and their synergistic analysis at different
45 frequencies. The dual-polarization upgrade of the United States National Weather Service (NWS) S-band Weather
46 Surveillance Radar 1988 Doppler (WSR-88D) network was completed in 2013. Germany finished upgrading its C-band
47 network to polarimetry in 2015 in parallel with other European countries. The synergistic exploitation of polarimetric
48 precipitation radars together with measurements from cloud radars and other instrumentation available at supersites and
49 research institutions enables for the first time a thorough evaluation and potential improvement of current microphysical
50 parameterizations based on detailed multi-frequency remote-sensing observations. Data assimilation merges observations and
51 models for state estimation as a prerequisite for prediction and can be seen as a smart interpolation between observations while
52 exploiting the physical consistency of atmospheric models as mathematical constraints.

53 Considerable knowledge gaps still exist, however, both in radar polarimetry and atmospheric models, which still impede the
54 full exploitation of the triangle between radar polarimetry, atmospheric models, and data assimilation and call for a coordinated
55 interdisciplinary effort. The German Research Foundation (Deutsche Forschungsgemeinschaft, DFG) responded to this call
56 and established the Priority Program "Polarimetric Radar Observations meet Atmospheric Modelling (PROM)"; its first 3-
57 year funding period began in 2019, which will be followed by a second funding period starting in 2022. PROM exploits the
58 synergy of polarimetric radar observations and state-of-the-art atmospheric models to better understand moist processes in the
59 atmosphere, and to improve their representation in climate- and weather prediction models. The overarching goal is to extend
60 our scientific understanding at the verges of the three disciplines, radar polarimetry – atmospheric models – data assimilation,
61 for better predictions of precipitating cloud systems. To approach this goal the initiators of PROM at the Universities of Bonn
62 and Leipzig in Germany identified the following five objectives (see also Trömel et al., 2018):

63 1) Exploitation of radar polarimetry for quantitative process detection in precipitating clouds and for model evaluation
64 including a quantitative analysis of polarimetric fingerprints and microphysical retrievals,

65 2) iImprovement of cloud and precipitation schemes in atmospheric models based on process fingerprints detectable in
66 polarimetric observations,

67 3) mMonitoring of the energy budget evolution due to phase changes in the cloudy, precipitating atmosphere for a better
68 understanding of its dynamics,

69 4) aAnalyzing precipitation system by assimilation of polarimetric radar observations into atmospheric models for weather
70 forecasting, and

71 5) rRadar-based detection of the initiation of convection for the improvement of thunderstorm prediction.

72 In the first funding period, each of the 14 projects (see https://www2.meteo.uni-bonn.de/spp2115) distributed over Germany
73 contribute to at least one of these objectives. In most projects, a radar meteorologist works together with a modeller in order
74 to successfully combine expert knowledge from both research fields. This overview article of the ACP/AMT/GMD inter-
75 journal special issue entitled "Fusion of radar polarimetry and numerical atmospheric modelling towards an improved
76 understanding of cloud and precipitation processes" outlines methodologies developed and results achieved from a selection
77 of the projects during the past two years, and provides overall perspectives for the next four years. The paper is organized as
78 follows: Section 2 explains prevailing challenges in the representation of clouds in atmospheric models, while Sect. 3 provides
79 methodologies to extend our insight in the microphysics of clouds and precipitation by exploiting radar polarimetry. Section 4
80 addresses the fusion of numerical modelling and radar polarimetry via model evaluation either in radar observation space using
81 observation operators or using microphysical retrievals. First conclusions for improved model parameterizations and for a
82 better representation of model uncertainty in radar data assimilation are drawn. Section 5 provides a summary and perspectives
83 for the following years.

84 **2 Representation of clouds in atmospheric models**

85 The representation of cloud and precipitation processes in atmospheric models is a central challenge for NWP and climate
86 projections (e.g., Bauer et al., 2015; Forster et al., 2021), which also impacts offline hydrological models by modulating the
87 distribution of incoming solar radiation and precipitation and affecting the simulated hydrological processes such as
88 evapotranspiration, runoff, and groundwater depths (e.g., Shrestha, 2021). While the primitive equations provide a solid
89 theoretical basis for atmospheric model dynamics, the key diabatic processes that drive energetics and thus circulation, are
90 poorly resolved. Important diabatic processes are linked to cloud and precipitation microphysics acting at scales of
91 micrometres and turbulent processes ranging from several to hundreds of meters. While significant progress has been achieved
92 by high-resolution modelling at the coarser end of this range (e.g., Heinze et al., 2017; Stevens et al., 2020), the intricate and
93 complex microphysical processes still require parameterizations in any dynamic atmospheric model down to and including the
94 scale of direct numerical simulations (e.g., Mellado et al., 2009).

95 A key uncertainty in weather prediction and climate modelling results from the still-rudimentary representation of moist
96 processes and from the diabatic heating/cooling the models induce due to latent heat and their interaction with radiation. The
97 generation and interpretation of past and future climate states additionally has to consider changes in microphysical processes
98 due to anthropogenic aerosol acting, e.g., as cloud condensation nuclei and ice nucleating particles. For short-term weather
99 prediction, the location and evolution of convective events with lifetimes of hours or less are particularly challenging, while
100 relatively slow moving and frontal systems with lifetimes of days show reasonable predictability (Alifieri et al., 2012).

101 Atmospheric modelling in Germany has recently seen substantial advances both in terms of cloud-resolving simulations in
102 NWP mode and in the implementation of ice and mixed-phase precipitation formation processes. Traditionally, different model
103 systems were used for NWP and climate modelling, which were also both heavily used in academic research. The modelling
104 system for long-term climate integrations is the ECHAM model (Stevens et al., 2013). Since it was created by modifying
105 global forecast models developed by ECMWF (European Centre for Medium-Range Weather Forecasts), its name is a
106 combination of ECMWF and Hamburg, the place of development of its parameterization package. The COSMO model,
107 however, was operated at horizontal resolutions down to 2.8 km and used for NWP and reanalysis studies. Research with the
108 ECHAM (the acronym is a combination of ECMWF (European Centre for Medium-Range Weather Forecasts) and Hamburg)
109 model family originating from the NWP model of the ECMWF focused on long-term climate integrations at horizontal
110 resolutions on the order of 100 km (Stevens et al., 2013), and the COSMO model operated at horizontal resolutions down to
111 2.8 km was used for NWP and reanalysis studies. Both model families are currently being replaced by the ICOsahedral
112 Nonhydrostatic (ICON) modelling framework (Zängl et al., 2015) jointly developed by the Max-Planck Institute for
113 Meteorology and the German national meteorological service (Deutscher Wetterdienst, DWD). Its climate version (the ICON
114 general circulation model, ICON GCM) inherited its physics package from the ECHAM model, and the NWP version
115 incorporated the one from the COSMO model. A third version largely based on the COSMO physics package was developed
116 for higher resolutions (Dipankar et al., 2015) and employs a large-eddy turbulence scheme (ICON-LEM). The latter is able to
117 operate on large domains (Heinze et al., 2017; Stevens et al., 2020) and includes aerosol-cloud interactions (Costa-Surós et al.,
118 2020). In PROM primarily the three ICON model variants (ICON-LEM, ICON-NWP, and ICON-A/GCM) are used.

119 In most atmospheric models, cloud and precipitation microphysical processes are represented by bulk microphysical schemes
120 that distinguish between different hydrometeor classes and include their specific masses as prognostic variables while their
121 size distributions are parameterized (the ICON model considered here uses the scheme by Seifert and Beheng, 2006).
122 Computationally much more demanding are so-called spectral-bin microphysics schemes (Khain et al., 2015), which evolve
123 cloud- and precipitation particle size distributions discretized into size-interval bins. An example is the Hebrew University
124 Cloud Model (HUCM) created by Khain et al. (2005) that treats both liquid and much more intricate (since ice may occur in
125 various shapes and densities) ice crystal distributions. The model is employed by some of the PROM projects in addition to
126 the liquid-only bin-microphysics model by Simmel et al. (2015) extended to the ice phase based on the scheme by Hashino

127 and Tripoli (2007). For the simulation of the evolution of specific air volumes a Lagrangian particle model (McSnow; Brdar
128 and Seifert, 2018) is used in PROM, that models ice and mixed-phase microphysical processes such as depositional growth,
129 aggregation, riming, secondary ice generation, and melting closer to the real processes than bulk formulations. Microphysical
130 processes including radiation-particle interactions obviously depend on particle shape; thus, the evolution of shapes in particle
131 models – and their signatures in radar observations – is instrumental for a full understanding and adequate representation of
132 the microphysical processes in models. Advanced microphysical parameterizations such as spectral-bin or Lagrangian particle
133 schemes are relevant for cloud-resolving models and exploited in PROM for the development and improvement of bulk
134 parameterizations. Scientific questions about global climate require long model integrations and thus coarse spatial resolutions
135 due to computing time constraints. At these resolutions (usually of order of 100 x 100 km² in the horizontal), fractional
136 cloudiness needs to be considered when the grid-box mean relative humidity is below 100%, which requires parameterizations
137 of subgrid-scale variability in relative humidity. Here, PROM builds on assumptions employed in the global ICON model
138 (ICON GCM) to predict fractional cloudiness (e.g., Quaas, 2012).

3 Observational insights from polarimetric radar observations and challenges

140 DWD operates 17 state-of-the-art polarimetric Doppler C-band weather radars which provide a 3-D sampling of precipitating
141 particles above Germany every five minutes. Together with their Doppler information, radars are the backbone for precipitation
142 and nowcasting products for all meteorological services. Although precipitation monitoring is still the most widespread
143 application of weather radars, their upgrade to polarimetry worldwide not only improves precipitation estimates; their
144 observations are also increasingly exploited for the evaluation and improvement of the representation of cloud- and
145 precipitation processes in atmospheric models (e.g., Gao et al., 2011; Jung et al., 2012; You et al., 2020; Wang et al., 2020).
146 Additional observations from cloud radars nowadays available at so-called supersites (in Germany e.g., the Jülich Observatory
147 for Cloud Evolution – Core Facility; JOYCE-CF; Löhnert et al., 2015; http://www.cpex-lab.de), universities, and research
148 facilities (e.g. the Leipzig Aerosol and Cloud Remote Observations System; LACROS; Bühl et al., 2013) open- opportunities
149 to inform and improve atmospheric models. The use of shorter wavelengths of cloud radars shifts the sensitivity of the
150 observations towards smaller particles and partly increases the magnitude of the received polarimetric signals (e.g. K_{DP} – the
151 differential phase shift between horizontal and vertical polarization per distance called specific differential phase – scales with
152 λ^{-1}), which allows for more detailed studies of ice and cloud microphysics. Polarimetric and multi-frequency radar observations
153 allow for a more granular look at microphysical processes and provide a great data base for model evaluation, the improvement
154 of microphysical parameterizations, and data assimilation, and thus have the potential to significantly improve both weather
155 forecasts and climate predictions.

3.1 Multi-frequency and spectral polarimetry for ice and cloud microphysics

The PROM-project *Understanding Ice Microphysical Processes by combining multi-frequency and spectral Radar polarImetry aNd super-parTicle modelling (IMPRINT)* improves ice microphysical process understanding by using spectral multi-frequency and radar polarimetric observations in combination with Monte-Carlo Lagrangian super-particle modeling (Brdar and Seifert, 2018). Mid-latitude stratiform clouds, which occur frequently during winter time over JOYCE-CF, are the main focus. Radar polarimetric variables are well known to be particularly sensitive to the presence of asymmetric ice particles (e.g. Kumjian, 2013). Only recently, also polarimetric cloud radars operating at Ka or W-band are routinely available (Oue et al., 2018; Myagkov et al., 2016; Bühl et al., 2016; Matrosov et al., 2012). Some polarimetric variables are wavelength dependent (K_{DP} is inversely proportional to the wavelength), which provides enhanced sensitivity to ice particle concentration at higher frequencies. Multi-frequency approaches are complementary to radar polarimetry as they are sensitive to larger ice particles. Most commonly, the dual wavelength ratio (DWR), defined as the logarithmic difference of the effective reflectivity Z_e at two frequencies, is used. When ice particles transition from Rayleigh into non-Rayleigh scattering from one wavelength to a higher one, the DWR increases, which allows ~~to infer~~inferring the characteristic size of the underlying size distribution. The use of three radar frequencies (e.g. X, Ka,W) extends the discernable size range; e.g. the DWR of the Ka-W combination saturates for very large particles (Kneifel et al., 2015; Ori et al., 2021). The information content can be further extended when also the Doppler spectral information is explored. The different fall velocities allow for the separation of different hydrometeors; the high differential reflectivity (Z_{DR}) signal originating from small, slow falling ice crystals can be ~~distingished~~distinguished from the also low Z_{DR} signal of faster falling snow aggregates, which usually dominate the total Z_{DR}. Only few studies used so far spectral polarimetric observations for ice and snow microphysical studies (Luke et al., 2021; Oue et al., 2018; Pfitzenmayer et al., 2018; Spek et al., 2008). The observations collected during the first multi-months winter campaign carried out at JOYCE-CF as part of the IMPRINT project provide for the first time the opportunity to investigate both, polarimetry and multi-frequency observations in the Doppler spectra space. An example is the analysis of the dendritic growth layer (DGL) illustrated in Fig. 1 for a snowfall event observed on 22~~nd~~ January 2019 at JOYCE-CF. Especially in the upper half of the cloud, ~~the~~ Z_{DR} is enhanced while K_{DP} values are low (Fig. 1b-c). Starting at the -15 °C isotherm, ~~the~~ Z_{DR} sharply decreases and shows an anti-correlation ~~to~~ with the enhanced DWR (Fig. 1a) and K_{DP} values. These polarimetric signatures have been reported by previous studies (e.g., Moisseev et al., 2015 among others), and also the DWR increase below the -15°C level resembles the examples shown in Oue et al. (2018). Oue et al. (2018) concluded in agreement with findings in Moisseev et al. (2015), that an increasing concentration of asymmetric aggregates ~~are~~is partly responsible for ~~the~~ enhanced K_{DP} values ~~of K_{DP}~~ because the number of small ice particles ~~will~~ decrease due to aggregation. The spectrally-resolved Z_{DR} (sZ_{DR}, Fig. 1e), however, reveals that high Z_{DR} producing, slowly falling ice particles are still present down to the -5 °C level. The spectrally resolved DWR (Fig. 1d) shows that the particles falling from above into the DGL are already partly aggregated. At -17 °C, the spectra are much wider and a new spectral mode appears which is linked to the rapid sZ_{DR} increase (Fig. 1e). The new ice particle mode increases in Doppler velocity and sDWR until 20 dB are reached. Unlike Z_{DR}, ~~the~~ K_{DP} (Fig. 1c and

189 f) remains at values between 1 and 2 °/deg km^{-1} down to the -5 °C level. A possible explanation of the bimodal spectra -

190 increased sZ$_{DR}$ and K$_{DP}$ might be secondary ice processes such as collisional fragmentation (Field et al., 2017). The few

191 existing laboratory studies indicate that the number of fragments rapidly increases at -20 °C, reaching a maximum at -17 °C

192 and decreasing again towards -10 °C (Takahashi et al., 1995; Takahashi, 2014). This temperature dependence fits well to the

193 observed radar signatures in the DGL, although the laboratory studies only considered collisions of solid ice spheres. As we

194 can exclude strongly rimed particles in the snowfall case shown in Fig. 1, fragile dendritic structures growing on the surface

195 of aggregates might be responsible, which precipitate into the DGL and might easily break into smaller pieces during particle

196 collisions (Fig. 1d). Monte-Carlo Lagrangian super-particle model (Brdar and Seifert, 2018) simulations were recently

197 extended in IMPRINT by a habit prediction scheme and a parameterization of ice collisional fragmentation following Phillips

198 et al. (2017). The role of ice fragmentation and other ice microphysical processes is currently investigated with a radar

199 observation operator for explaining the observed radar signatures of intense aggregation shown in Fig. 1.

200

201 The PROM-project *Investigation of the initiation of convection and the evolution of precipitation using simulations and*

202 *polarimetric radar observations at C- and Ka-band (IcePolCKa)* combines observations of the C-band Polarization Diversity

203 Doppler Radar (POLDIRAD) at the German Aerospace Center (DLR), Oberpfaffenhofen, with those of the Ka-band,

204 Milimeter-wave cloud RAdar of the Munich Aerosol Cloud Scanner (miraMACS) at Ludwig-Maximilians-Universität (LMU),

205 Munich. While IMPRINT combines triple-frequency zenith-pointing observations with spectral cloud radar polarimetry,

206 IcePolCKa explores the life cycle of convective precipitation with spatially separated weather and cloud radars in order to

207 quantify ice crystal properties in precipitation formation. The project focuses on ice particle growth and its role in precipitation

208 formation within convective cells. Coordinated Range-Height-Indicator (RHI, varying elevation at constant azimuth) scans

209 along the 23 km long cross-section between both radars allow to observe DWR (Fig. 2a) and Z$_{DR}$ (Fig. 2b) fingerprints of

210 individual convective cells. While the deviation from Rayleigh scattering with increasing ice crystal size at the cloud radar

211 wavelength is used toallows distinguishing regions dominated by aggregation from regions with depositional growth, the

212 slanted perspective of the weather radar helps to narrow down the aspect ratio of ice crystals. Although the DWR technique to

213 infer ice crystal size is well establishedwell established (e.g. Kneifel et al., 2015), assumptions about the unknown ice crystal

214 shape are necessary. Here, simultaneous polarimetric measurements, like Z$_{DR}$, help to narrow down estimates of the average

215 asphericity of ice crystals and reduce ambiguities in retrieving ice crystal size and ice water content. IcePolCKa develops an

216 algorithm, which uses Z$_H$, Z$_{DR}$ and DWR measurements from the two radars to retrieve IWC, the mean particle diameter D$_m$,

217 and the aspect ratio of ice crystals using a least-squares fit between measurements and T-matrix scattering simulations. The

218 model of horizontally aligned spheroids in combination with an effective medium approximation following Hogan et al (2012)

219 is used to find the simplest ice particle model which explains the multi-wavelength polarimetric measurements. The approach

220 allows to studystudying the covariance of DWR and Z$_{DR}$ while varying particle density, mean particle diameter D$_m$, and aspect

221 ratio. More sophisticated models, such as discrete dipole approximation (DDA) simulations of specific ice crystals, would

222 require the knowledge of the aspect ratio, and make it hard to identify ice shape collections along these free variables. The

multi-wavelength polarimetric measurements are also used as a benchmark for convective precipitation formation in NWP models, where cloud microphysics introduce substantial uncertainty (e.g. Morrison et al., 2020; Xue et al., 2017). In IMPRINT simulated microphysical processes in NWP models will be compared to fingerprints in radar observations: A nested WRF setup covering the overlap area of both radars is used to simulate convective events with microphysical schemes of varying complexity while the Cloud-resolving model Radar SIMulator (CR-SIM; Oue et al., 2020), produces synthetic radar observations, such as DWR (Fig. 2c) and Z_{DR} (Fig. 2d). Fig. 2 illustrates that the Predicted Particle Properties (P3) scheme (Morrison and Milbrandt, 2015) is able to produce DWR features of similar magnitude and variability compared to the observations, while a realistic ice particle asphericity is still missing. IcePolCKa compiled over 30 convective days of polarimetric measurements and simulations with 5 different schemes over a 2-year period, which is currently used to analyse how well these different microphysical schemes reproduce the polarimetric observations. A cell-tracking algorithm (TINT; Fridlind et al., 2019) facilitates the comparison on a cell object basis. Comparison of macrophysical cloud characteristics, such as echo top height or maximum cell reflectivity, show that the model simulates too few weak and small-scale convective cells, independent of the microphysics scheme. In ongoing studies, the P3 scheme seems to better represent radar signatures within the ice phase, while a spectral bin scheme tends to better simulate radar signatures within rain, where all other schemes are not able to correctly reproduce observed Z_{DR} features.

The PROM-project *A seamless column of the precipitation process from mixed-phase clouds employing data from a polarimetric C-band radar, a micro-rain radar and disdrometers (HydroColumn)* characterizes precipitation processes inside a vertical atmospheric column by combining polarimetric Doppler weather radar observations with co-located measurements from micro-rain radars, disdrometers and in-situ measurements, and by relating these observations to the large-scale atmospheric thermodynamics derived from NWP models. To date, spectral analyses are mostly performed with cloud radars operating at shorter wavelengths (see previous paragraphs or, e.g., Shupe et al., 2004; Verlinde et al., 2013; Kalesse et al., 2016; Gehring et al., 2020; Li and Moisseev, 2020), but their implementation across the national C-band radar network offers prospects for operational area-wide applications, e.g. the identification of dominant precipitation particle growth processes such as aggregation or riming. While the operational DWD birdbath scan has so far been used primarily to monitor Z_{DR} (Frech and Hubbert, 2020), *HydroColumn* now also exploits the Doppler spectra measured at C-band for the analysis of microphysical process information. Fig. 3 shows quasi-vertical profiles (QVPs; Trömel et al., 2014; Ryzhkov et al., 2016) of polarimetric variables and Doppler spectra from birdbath scans for a stratiform precipitation event monitored with the Hohenpeißenberg C-band research radar (47.8014N, 11.0097E) of DWD together with in-situ particle images obtained by the Falcon research aircraft from DLR during the BLUESKY campaign (Voigt et al., 2021) within the *POLICE* project (Sect.4.2.1). In-situ measurements have been performed with the Cloud, Aerosol and Precipitation Probe CAPS (Kleine et al., 2018) integrated in a wing station on the Falcon flying within a horizontal distance of about 20 km from the radar site and within about ±15 min of the radar measurements. The dendritic growth layer (DGL; Ryzhkov and Zrnic, 2019) centered around

257 -15 °C is characterized by Z_{DR} maxima of ~ 1 dB and K_{DP} of ~ 0.2 ~~°~~ deg km^{-1}, and a strong Z_H increase towards lower levels

258 (Fig. 3a). Particle images collected at temperatures below about -15 °C indicate mostly small irregular ice particles with the

259 number of larger particles increasing toward -15 °C (see levels L1 and L2 in Fig. 3c), and further down also reveal dendrites

260 and plates (L3, L4). In general, aggregation and riming become highly effective particle growth mechanisms at temperatures

261 around -7 °C (Libbrecht, 2005), and both processes result in a reduction of Z_{DR} (Fig. 3a). The vertically pointing Doppler

262 measurements can be used here to gain a deeper insight into the particle growth process. In this case study, the Doppler

263 measurements illustrated in Fig. 3b indicate typical ice-particle fall speeds increasing to about 2 m s^{-1} just above the melting

264 layer and thus suggest a transition from predominantly aggregates to moderately rimed particles based on the relationship

265 between Doppler velocity and riming degree found by Kneifel and Moisseev (2020). This conclusion is supported by the

266 corresponding in-situ images showing increasing riming of polycrystals and aggregates toward the melting layer (L6). The

267 analysis confirms the benefit of interpreting radar signatures from polarimetric weather radar observations in combination with

268 vertically pointing Doppler radar measurements, which was previously pointed out for higher-frequency cloud research radars

269 (Oue et al., 2018; Kumjian et al., 2020). This novel application of radar spectral analysis to vertically-pointing operational

270 weather radar scans may provide a more detailed view into intense precipitation events, such as hailstorms, where the use of

271 cloud radars is severely limited due to the strong attenuation at high radar frequencies.

272 **3.2. Anthropogenic modifications of precipitation microphysics**

273 The PROM-project ***Polarimetry Influenced by CCN aNd INP in Cyprus and Chile (PICNICC)*** seeks to improve our

274 understanding of aerosol effects on microphysical growth processes in mixed-phase clouds. ***PICNICC*** exploits unique remote-

275 sensing datasets from the LACROS suite (Radenz et al., 2021) extended with ground-based remote sensing instruments

276 installed at Leipzig University, Universidad de Magallanes (Punta Arenas), and Cyprus University of Technology (Limassol).

277 Thus, dual-frequency polarimetric radar observations from the polluted, aerosol-burden Northern and from the clean, pristine

278 Southern hemisphere can be contrasted for microphysical process studies as already performed in the project for stratiform

279 mixed-phase clouds to investigate inter-hemispheric contrasts in the efficiency of heterogeneous ice formation (Radenz et al.,

280 2021). The PICNICC project challenges the hypothesis that higher ice crystal concentrations favour aggregation, which is

281 expected to be more frequent for high aerosol loads and accordingly higher ice nucleating particle (INP) concentrations, while

282 riming should prevail when supercooled liquid layers are sustained due to a scarcity of INP. Evaluating this hypothesis requires

283 the distinction between aggregation and riming in mixed-phase cloud systems. Fig. 4 demonstrates for a deep mixed-phase

284 cloud system passing the low-aerosol site in Punta Arenas (53°S, 71°W), Chile, on 30 August 2019, the capability of the

285 LACROS suite ~~when combined with a 94-GHz Doppler radar~~ to distinguish between aggregates and rimed particles when

286 combined with a 94-GHz Doppler radar. The pattern of the 94-GHz radar reflectivity factor (Z_e, Fig. 4a) underlines the complex

287 structure of the system. The height spectrogram of the vertical-pointing 94-GHz slanted linear depolarization ratio (SLDR,

288 Fig. 4 e) from 08:30 UTC exhibits regions of changing shape signatures and multi-modality in the cloud radar Doppler spectra,

289 where multiple hydrometeor populations coexist. The polarizability ratio ξ_e (Myagkov et al., 2016; ~~) (~~Fig. 4d) obtained from

290 the RHI scans of SLDR and the co-cross correlation coefficient of horizontal and vertically polarized channels in the slanted

291 basis ρ$_x$ at 35 GHz (Fig. 4 b, c) ~~is obtained~~ allows to estimate a density-weighted hydrometeor shape. SLDR is more suited

292 for shape classification compared to LDR. By slanting the polarization basis by 45 $°$, ~~deg,~~ the returned LDR signatures are

293 much less sensitive to the canting angle distribution of the targets, especially at low elevation angles (Matrosov et al., 2001;

294 Myagkov et al., 2016). The polarimetric RHI scans and the Doppler spectra data enable the retrieval of the vertical profile of

295 the hydrometeors: Columnar-shaped bullet rosettes are formed between 2.5 km height and cloud top as indicated in the RHI

296 scans by an elevation-constant SLDR (Fig. 4b) and an increase of ρ$_x$ with decreasing elevation (Fig. 4c). ξ$_x$ values around 1.3

297 (Fig. 4d) ~~is~~ are characteristic for slightly columnar crystals. The decreasing elevation-dependence of ρ$_x$ already at around 3 km

298 height (-15 to -20°C) suggests more random particle orientations; here the W-band SLDR spectra (Fig. 4e) show reduced

299 values, likely due to the co-existence of dendritic ice crystals, which are formed preferably in this temperature range. The co-

300 location of dendrites and columnar crystals can be explained by either splintering of the arms of the dendritic crystals or a

301 mixing of locally produced dendrites with columnar crystals from higher up, or both. Below 2.5 km, ξ$_x$ decreases toward unity,

302 indicating the growth of isometric particles. ~~Also~~ In addition, the vertical-pointing W-~~b~~Band SLDR slowly decreases toward

303 the cloud base, while fall velocities increase (Fig. 4e). Both features are characteristic for riming, which is corroborated by co-

304 located lidar observations that indicate liquid water in the cloud-base region (not shown). Doppler spectra profiles such as the

305 one presented in Fig. 4e are also used in a new neural-network-based riming detection algorithm recently tailored by Vogl. et

306 al. (2021) for vertical-pointing cloud radar observations. This new approach is insensitive to the mean Doppler velocity, which

307 is - especially at Punta Arenas - strongly influenced by orographic mountain waves, because the radar reflectivity factor,

308 skewness and the edge width of the Doppler spectrum is used instead.

309

310 The PROM-project *Investigating the impact of Land-use and land-cover change on Aerosol-Cloud-precipitation*

311 *interactions using Polarimetric Radar retrievals (ILACPR) analyzes* polarimetric radar observations and model simulations

312 simultaneous~~ly~~ in order to improve our understanding of~~~~ land-aerosol-cloud-precipitation interactions. The Terrestrial Systems

313 Modelling Platform (TSMP; Shrestha et al., 2014; Gasper et al., 2014) developed under the DFG-funded Transregional

314 Research Center TR32 (Simmer et al., 2015) is used ~~t~~to simulate summertime convective storms passing the polarimetric X-

315 band radar (BoXPol, e.g. Diederich et al., 2015a,b) located ~~in~~over Bonn, Germany. TSMP generally underestimates the

316 convective area fraction, high reflectivities, and the width/magnitude of differential reflectivity (Z$_{DR}$) columns indicative of

317 updrafts, all leading to an underestimation of the frequency distribution for high precipitation values (Shrestha et al., 2021a).

318 A decadal scale simulation over the region using the hydrological component of T~~S~~MS~~P~~ also shows that much of the variability

319 in the simulated seasonal cycle of shallow groundwater could be linked to the distribution of clouds and vegetation (Shrestha,

320 2021), which further emphasizes the importance of ~~model~~ evaluati~~ng~~on ~~in~~ the represent~~ation of~~ing clouds and precipitation in

321 numerical models. The fusion of radar observations and models with the aid of observation operators~~,~~ allows for an extended

322 interrogation of the effects of anthropogenic interventions on precipitation generating processes and the capabilities of

323 numerical models to reproduce them. Here, findings from one simulated hailstorm observed on 5 July 2015 passing the city of

Bonn, Germany, are explained. Sensitivity simulations are conducted using large-scale aerosol perturbations and different land-cover types reflecting actual, reduced and enhanced human disturbances. While the differences in modelled precipitation in response to the prescribed forcing are below 5 %, the micro- and macrophysical pathways ~~are found to~~ differ, acting as a buffered system to the prescribed forcings (Stevens and Feingold, 2009; Seifert and Beheng, 2012). Fig. 5 shows vertical cross-sections reconstructed from volume scans measured with BoXPol together with simulated Z_H and Z_{DR} for the TSMP simulations with actual land-cover but perturbed condensation nuclei (CN) and ice nucleating particle (INP) concentrations. CN concentrations are 100 cm^{-3} for maritime and 1700 cm^{-3} for continental aerosol. Similarly, default INP concentrations for dust, soot and organics are 162E3 m^3, 15E6 m^3 and 177E6 m^3, respectively, ~~for default INP~~. For low/high INP, the concentration of soot and organics are decreased/increased by one order of magnitude. To generate the synthetic radar observations the Bonn Polarimetric Radar observation Operator, B-PRO, (Xie et al., 2021; Xie et al., 2016; Heinze et al., 2017; Shrestha et al., 2021b) is applied. B-PRO is based on the non-polarimetric version of EMVORADO (Zeng et al., 2016); its code part for computing unattenuated radar reflectivity on the original model grid (Blahak, 2016) has been expanded to unattenuated polarimetric variables based on spheroidal shape assumptions (T-matrix). Because the full polarimetric version of EMVORADO (Pol-EMVORADO, see Section 4.1) was only released very recently, the model data in ILACPR has been processed using B-PRO. Preliminary comparisons between B-PRO and Pol-EMVORADO (not shown here) exhibit negligible differences in their results on the model grid, but Pol-EMVORADO is much more computationally efficient and takes effects of beam broadening and attenuation along the actual radar ray paths into account. The vertical cross sections are compared at different times marked by the vertical grey bars in the time series of Convective Area Fraction (CAF, Fig. 5 a), defined as the ratio of area with $Z_H > 40$ dBZ (at 2 km a.g.l.) to total storm area. On average BoXPol observations show a bit higher CAF compared to the simulations. The evolution is always similar in terms of an initial increase and intensification in the second part of the observation period, where the experiment with maritime aerosols and low INP (Mar-lowIn) is closest to the observations. All simulations show Z_H and Z_{DR} patterns comparable to BoXPol observations, however, the experiment with continental aerosol and default INP (Con-defIN, Fig. 5c) shows weaker Z_H, while Mar-lowIN (Fig. 5d) shows somewhat higher Z_H values compared to BoXPol (see Fig 5a). The simulations with maritime CN produce low cloud droplet concentrations with larger mean diameters compared to the simulations with continental CN. Accompanied by a very strong updraft, this also leads to high concentrations of supercooled raindrops above the melting layer with broader spatial extent (due to a broader updraft region) compared to the simulations with continental CN and contributes to an enhanced growth of hail resulting in higher Z_H. Also, as shown in the CAF time -series ~~of the CAF~~, simulations with continental aerosol and default/high IN tend to exhibit similar behaviour in radar space, with the latter exhibiting higher CAF only at latter stages of the storm. The continental CN simulations with default and high IN differ in terms of simulated updraft speed and total hydrometeor content, being higher for the latter one. However, Cont-highIN produces smaller graupel and hail particles compared to Cont-defIN, resulting in similar Z_H. The experiment with continental aerosol and high INP concentration (Con-highIN, not shown) generates similar polarimetric moments to Con-lowIN. All experiments exhibit vertically extensive columns of (slightly) enhanced Z_{DR}, collocated with intense simulated updrafts reaching up to 13 to 14 km. Indeed, Z_{DR} columns emerged ~~recently~~ as proxies for

358 updraft strength and ensuing precipitation enhancement (Weissmann et al., 2014; Simmer et al., 2014; Kumjian et al., 2014;
359 Kuster et al., 2020), and research on their exploitation for nowcasting and data assimilation is ongoing. In Fig. 5c/d synthetic
360 Z_{DR} columns are vertically extensive, while Z_{DR} values within the column stay below 0.3 dB. BoXPol observations show Z_{DR}
361 columns reaching up to 6 km height only but with Z_{DR} values exceeding 1dB. While Z_{DR} values in the lower part of the columns
362 are mostly generated by large raindrops, freezing drops and wet hail determine Z_{DR} in the upper parts of the column (Kumjian
363 et al., 2014; Snyder et al., 2015). The diverging appearance of observed and synthetic Z_{DR} columns may point to deficiencies
364 in the treatment of raindrops undergoing freezing and motivates further research. Too rapid freezing of drops combined with
365 graupel generated from the frozen drops may generate enhanced but still low Z_{DR} up to high altitudes. Following Ilotoviz et
366 al. (2018) such attributes of Z_{DR} columns are highly determined by the vertical velocity, hail size, and aerosol concentration,
367 e.g. higher CN concentrations lead to higher columns with higher Z_{DR} values inside and also higher Z_H. In this case study and
368 the specific time step shown, Mar-lowIN (i.e. with lower CN concentration) shows a wider and somewhat taller Z_{DR} column
369 together with a more intense Z_H core (compare Fig. 5c/d). Further explanations require an improved representation of the Z_{DR}
370 columns in the model.

371 **4 Fusion of radar polarimetry and atmospheric models**

372 Probably the most important and central tool for connecting polarimetric observations with numerical atmospheric models are
373 observation operators, which generate virtual observations from the model state. These virtual observations can be directly
374 compared with the real observations and signatures of microphysical processes including their temporal evolution. Thus, the
375 accuracy of precipitation and cloud parameterizations can be indirectly evaluated and a database established for model
376 optimization. Missing polarimetric process fingerprints (e.g. Kumjian, 2012) in the virtual observations may hint at model
377 deficiencies, and model parameterizations can be adapted in order to increase the coherence between real and virtual
378 observations. Moreover, sufficiently accurate and fast observation operators are mandatory for the direct assimilation of
379 observations using ensemble methods.
380 However, bulk cloud microphysical parameterizations required for NWP models include assumptions on several critical
381 parameters and processes which are not explicitly prognosed ~~respectively~~ or resolved by the governing numerical model. An
382 example are the inherently assumed particle size distributions and their relations to the prognostic moments (hydrometeor mass
383 and number densities). Another challenge is the handling of hydrometeor parameters that are not or only insufficiently
384 constrained~~are insufficiently or not at all constrained~~ by the model's microphysics but are highly relevant for the calculation
385 of virtual observations in the (radar) observation operator. For example, the melting state as well as shape, microstructure, and
386 spatial orientation of the different hydrometeors are not prognostic (or not even implicitly assumed) in most operational bulk
387 schemes. Therefore, suitable assumptions ~~need to be made~~are required in observation operators in order to compute meaningful
388 virtual observations. Moreover, bulk cloud microphysical schemes may only insufficiently approximate the natural variability,
389 and the interactions between the few assumed hydrometeor classes and the size distribution moments are mainly tuned to get,

390 e.g., the surface precipitation right. The current approximations in both numerical models and observation operators may hence
391 translate into different sources of errors and biases of the simulated radar variables (e.g. Schinagl et al., 2019; Shrestha et al.,
392 2021b). As an example, Fig. 7 shows too low polarimetric signals above the melting layer, which are partly caused by
393 assumptions inherent in the observation operator (see Sect. 4.2.1). Such problems challenge both model evaluation and data
394 assimilation. The Accordingly, central science questions are thereforeconcern the realism of the sensitivities of simulated radar
395 variables to parameters in the observation operators and the models as well as effective approaches to for the evaluation and
396 improvement of moist processes parameterizations.

397 Another challenge for large-scale applications such as long-term model evaluations or operational real-time data assimilation
398 based on large radar networks is the high computational demand and low speed of- current polarimetric radar observation
399 operators. Often, the operators apply some kind of pre-calculated lookup tables (LUT) of scattering properties and
400 parallelization techniques for speed optimizations (e.g. Wolfensberger and Berne, 2018; Matsui et al., 2019; Oue et al., 2020).
401 Despite that, radar simulations for a single timesteptime step take - depending on the computer - on the order of minutes for
402 one single plan position indicator (PPI) scan (Wolfensberger and Berne, 2018) or for a single model scene (CR-SIM; Oue et
403 al., 2020). Matsui et al. (2019) state the LUT generation process of their POLARRIS-f operator to only take a few minutes
404 when distributed to few thousands of processors, but do not elaborate on the required times for the actual simulation of the
405 radar measurement. The operator B-PRO (Xie et al., 2016), which uses neither of these techniques, is much slower, as
406 applications within SPP-PROM have demonstrated (Shresta et al., 2021b). While acceptable for research, real-time operational
407 applications may pose much stricter time constraints. Therefore, an important technical goal is to provide an efficient, yet
408 physically accurate and "state-of-the-art", polarimetric radar operator to the community, which reduces the simulation time
409 for multi-elevation PPI scans of many stations to a few seconds.

4.1 Polarimetric radar observation operator development

411 Within the PROM-project *Operation Hydrometeors,* the up-to-now non-polarimetric radar observation operator
412 EMVORADO (Zeng et al., 2016; Blahak and de Lozar, 2020; Blahak, 2016) has been extended to polarimetry (Mendrok et
413 al., 2021). (Non-polarimetric) EMVORADO has been designed to efficiently simulate PPI volume scan measurements of entire
414 radar networks from the prognostic model state of an NWP model for direct comparisons with the radar observations.
415 EMVORADO is part of the executable of both the COSMO and ICON NWP models, which allows to run the operator within
416 a NWP model run and to access the model state and radar variables in memory. The code is MPI- and OpenMP-parallelized
417 and thus fully exploits the computational power of modern HPCs and avoids storing and re-reading extensive model state data
418 to/from hard drives. This enables large-scale real-time applications such as operational data assimilation and extensive NWP
419 model verifications using whole radar networks at high temporal resolution. Its modular nature allows for relatively easy
420 interface development to other NWP models. An offline framework is also available, which accesses model states of one model
421 time step from hard disk. EMVORADO includes detailed modular schemes to simulate beam bending, beam broadening and
422 melting effects, and allows users to choose for each process between computationally cheap and physically accurate options.

423 The operator has been used for the assimilation of radar reflectivity with positive impact on precipitation forecasts (Bick et al.,
424 2016; Zeng et al., 2018, ; 2019, ; 2020). Currently, DWD uses EMVORADO to operationally assimilate 3D volumetric
425 reflectivity and radial wind observations of its C-bBand radar network. Key for this application is also the extensive use of
426 precomputed lookup tables that relate (Mie-theory based) bulk reflectivity directly to hydrometeor densities and temperature.
427 The effects of neglecting radar beam pattern and- broadening of hydrometeor fall speeds on data assimilation have been
428 investigated in a joint effort together with the PROM-project *Representing model error and observation Error uncertainty*
429 *for Data assimilation of POLarimetric radar measurements* (*REDPOL*) (Zeng et al., 2021a).
430 The polarimetry-extended EMVORADO, in the following referred to as Pol-EMVORADO, has inherited all features of
431 EMVORADO, which in turn have been expanded where necessary to calculate and handle polarimetric variables. This
432 includes, e.g., beam bending, beam broadening, and beam smoothing schemes, effective medium approximations allowing 1-
433 and 2-layered hydrometeors with different water-ice-air mixing schemes and melting topologies, and a lookup table approach
434 for an efficient access to polarimetric observables such as Z_{DR}, LDR, ρ_{HV}, and K_{DP}. Optionally, attenuation effects can be
435 considered, specific and differential attenuation (A_H and A_{DP}, respectively) provided, and further output quantities derivable
436 from the complex scattering amplitudes easily added. Pol-EMVORADO applies state-of-the-art scattering properties of
437 spheroidal particles derived by one-layered (Mishchenko, 2000) and two-layered T-Matrix approaches (Ryzhkov et al., 2011).
438 Assumptions on spheroid shape and orientation follow parameterizations introduced in Ryzhkov et al. (2011). The lookup
439 table approach has been revised to accommodate additional parameters necessary to derive the full set of polarimetric radar
440 output. For a given set of parameters affecting the hydrometeor scattering properties, the lookup tables are created only once,
441 stored in files, and re-used for subsequent runs.
442 Using pre-existing lookup tables, the computations for virtual polarimetric volume scans of radar networks are very fast. For
443 example, simulating the volume scans- observations of all polarimetric parameters for-of all 17 German radars takes a few
444 seconds only on a Linux workstation (8 cores) and adds only about 1 s per radar output time step to the model runtime when
445 performed online during a run of ICON-D2 (DWD's operational convection-allowing ICON version with 2 km grid spacing)
446 on DWD's NEC Aurora supercomputer. That is, simulating polarimetric radar data in intervals of 5 min as observed by DWD's
447 weather radar network adds up to-only a few percent of the total model runtime (Mendrok et al., 2021) making it possible to
448 runenabling the exploitation of Pol-EMVORADO for the assimilation of high temporal resolution polarimetric radar data in
449 an operational framework. Pol-EMVORADO has been- incorporated into the official version of EMVORADO and can be run
450 online (i.e. within a COSMO or ICON run) as well as offline (i.e. stand-alone with model fields from data files). Although
451 designed as a PPI volume scan observation operator for a radar network, its output can also be provided on NWP model grids.
452 An example of a Z_{DR} volume scan simulated by Pol-EMVORADO for the *REDPOL* project is shown in Fig. 6 (see also Sect.
453 4.2.3).
454 In summary, (Pol-)EMVORADO comprises a wide set of state-of-the-art features. While each of these features is provided
455 also by other observation operators, (Pol-)EMVORADO is, to our knowledge, unique in combining them into an-one operator
456 that allows to simulate virtual observations, including instrumental effects and in formats directly comparable to real

observational scans, from ~~within~~ NWP model runs in a comparably accurate and very fast manner targeted at operational applications. Mendrok et al. (2021) give a comprehensive description of the features developed or updated for Pol-EMVORADO including details on their implementation and performance.

However, ~~From~~ from the application of Pol-EMVORADO (or B-PRO, see Sect. 3.2) within PROM, a number of problems became evident. Modeling hydrometeors as homogeneous effective-medium particles (e.g. oblate spheroids) does not reproduce well the polarimetric signatures of low density hydrometeors like dendrites or aggregates typical for snow while keeping their microphysical properties (e.g. aspect ratio, degree of orientation) within realistic - observed or model-predicted - ranges and consistent between different radar frequencies. This deficiency has been demonstrated and explained from electromagnetic theory by Schrom et al. (2018). It is obvious in one case study (Shrestha et al., 2021b) and in Fig. 7, where Z_{DR} and K_{DP} in the snow-dominated layer between 2.5 and 5 km height almost entirely lack the typical observed features, i.e. bands of enhanced Z_{DR} and K_{DP} in the dendritic growth layer that then smoothly decrease to mostly positive, non-zero values towards the melting layer. This deficiency can also be observed with other polarimetric observation operators applying a T-matrix approach (see simulation-to-observation comparisons in Wolfensberger and Berne (2018), Matsui et al. (2019), Oue et al. (2020), where the lack of Z_{DR} and K_{DP} signatures is not discussed at all or exclusively explained by a lack of secondary ice, though), which nevertheless currently constitutes the state-of-the-art in radar polarimetry. Orientation and shape of frozen and melting hydrometeors are very variable, both in nature and in the assumptions used in observation operators, which translates into large uncertainties in polarimetric radar signatures (e.g., Matsui et al., 2019; Shrestha et al., 2021b).

To tackle these challenges, it is planned to interface Pol-EMVORADO to scattering databases or other scattering models in order to enable more realistic cloud ice and aggregate snowflake scattering properties and allow for improvements or extensions of the polarimetry-related microphysical assumptions (shape/habit/microstructure, orientation and their distribution, e.g., Wolfensberger et al., 2018), particularly for (partly-)frozen hydrometeors. For PROM's 2nd phase, we have proposed to take this up guided with Lagrangian particle model information as well as to test the application of Pol-EMVORADO in an operational data assimilation environment.

4.2 Model evaluation and improvements using forward simulations and microphysical retrievals

4.2.1 Convection-resolving simulations with COSMO

In a joint effort, the PROM-projects *Operation Hydrometeors* and *ILACPR* evaluate simulated stratiform precipitation events in radar observation space and develop a sophisticated polarimetry-based hydrometeor classification and quantification for the evaluation of the representation of hydrometeors in numerical models. Based on a stratiform event monitored on 7 October 2014 with the Bonn polarimetric X-~~b~~Band radar BoXPol, Fig. 7 illustrates the potential of using polarimetric observations for the evaluation and improvement of microphysical parameterizations. Fig. 7 a-f compare QVPs of measured and virtual Z_H, Z_{DR}, and K_{DP} with the Bonn Polarimetric Radar observation Operator B-PRO (Xie et al., 2021) to forecasts simulated with COSMO version 5.1 using its 2-moment cloud microphysics scheme (itype_gscp=2683; Seifert and Beheng, 2016). Due to a small spatial shift of the precipitation event in the simulations, the observations at 50.7305 N, 7.0717 E are compared with

simulations at a close-by grid point at 51.1 N, 7.0717 E. As demonstrated in Shrestha et al. (2021b) using a similar stratiform precipitation event, COSMO tends to simulate considerable amounts of melting graupel partly reaching the surface, which results in– higher synthetic Z_{DR} than observed (compare Fig. 7c/d) within and below the melting layer (ML). Above the ML, however, synthetic Z_{DR} already approaches 0 dB at around 6 km height, which indicates deficiencies in the ice-snow partitioning in COSMO as well as in the assumed snow morphology (soft spheroids) in the observation operator, both resulting in too low polarimetric signals. While the observed and simulated Z_H is comparable in terms of structure and magnitude - except a more pronounced observed ML - larger differences exist with respect to K_{DP} above the ML (Fig. 7e/f). While observations show bands of enhanced K_{DP} within the dendritic growth layer (DGL) centred around -15°C, the simulated K_{DP} is very weak indicating a lower crystal concentration of crystals and early aggregates compared to observations (e.g. Moisseev et al., 2015). Ice water content (IWC) above the ML retrieved from measured K_{DP} and differential reflectivity in linear scale Z_{dr}, i.e. IWC(K_{DP}, Z_{dr}) following Ryzhkov et al. (2018), agrees well with IWC modelled by COSMO in terms of structure, but has lower magnitudes (compare Fig. 7 g/h) in line with the lower simulated K_{DP}. Overall, Fig. 7 supports the hypothesis of a too strong graupel production in the simulations. *Operation Hydrometeors* also developed a robust radar-based hydrometeor classification (HMC) and mixing ratio quantification algorithm following Grazioli et al. (2015) and Besic et al. (2016, 2018) for the evaluation of the representation of hydrometeors in NWP models (standard output is the dominant hydrometeor type only). This HMC is based on clustering and has the advantage that the radar data are separated into clusters based on their polarimetric similarity (no theoretical preliminary calculation is needed), which are then identified as hydrometeor classes. Various clustering methods can be used here (e.g. Lukach et al. (2021)). The new method is relatively insensitive to uncertainties in the scattering properties of ice particles. Its application to the BoXPol observations above does not indicate graupel below the ML (Fig. 8a), while COSMO simulates a pronounced, thick graupel layer (Fig. 8b) including some melting graupel particles reaching the ground around at 1:45 UTC. Applying the HMC to the virtual observations, however, does not reproduce a graupel layer of similar intensity (Fig. 8c), probably caused by a too strong Z_H and temperature influence (compare with Fig. 7) relative to the polarimetric variables in the classification scheme which needs further investigation. A persistent challenge in according routines is that clusters are always separated by the 0 °C-level (e.g. Ribaud et al., 2019), i.e. hail or graupel are identified as clusters only below or above the melting layer. For the case study in Shrestha et al. (2021b) the simulated graupel layer was even more pronounced and sensitivity experiments were performed to guide model improvement: increasing the minimum critical particle diameter D_{crit}, which is required for self-collection of ice particles (aggregation) increased/improved the ice-snow partitioning, and a lower temperature threshold for snow and ice riming, T_{rime}, considerably reduced the graupel production.

Comparing state-of-the-art polarimetric retrievals of liquid water content (LWC), ice water content (IWC), particle number concentration N_t and mean particle diameter D_m (e.g. Ryzhkov et al., 2018; Ryzhkov and Zrnic, 2019; Bukovčić et al., 2020; Reimann et al., 2021; Trömel et al., 2019) with their simulated counterparts can also be used for evaluating NWP models and for data assimilation (Carlin et al., 2016). Fig. 7g/h, e.g., shows higher IWC(K_{DP}, Z_{dr}) than simulated by COSMO for the case study discussed earlier. However, For for more solid conclusions about possible model errors, as well as for the use of retrieved

524 quantities for data assimilation, the retrieval uncertainties must be estimated. The analysis of data collected in the ice regions
525 of tropical convective clouds indicates e.g., that IWC(K_{DP}, Z_{dr}) yields a root-mean-square error of 0.49 gm^{-3} with the bias
526 within 6% (Nguyen et al., 2017; 2019). Murphy et al. (2020) introduced the columnar vertical profile (CVP) methodology to
527 follow the track of research aircrafts and better co-locate in-situ data to radar microphysical retrievals. Applying the
528 methodology to two mesoscale convective systems, they found the best performance of polarimetric microphysical retrievals
529 in regions of high Z_{DR} and high K_{DP} but recommend a much larger dataset to ~~fully~~ finally conclude on the accuracy of these
530 retrievals.

531

532 The PROM-project ***POLarimetric signatures of ICE microphysical processes and their interpretation using in-situ***
533 ***observations and cloud modelling (POLICE)*** evaluates radar retrievals and models using in particular in-situ observations of
534 microphysical cloud parameters from the research aircrafts HALO (e.g. Wendisch et al., 2016; Voigt et al., 2017) and Falcon
535 (e.g. Voigt et al., 2010; Voigt et al., 2014; Flamant et al., 2017). Currently, ground-based polarimetric radar measurements and
536 aircraft in-situ data from the Olympic Mountain Experiment OLYMPEX (Houze et al., 2017; Heymsfield et al., 2018) are
537 exploited to investigate riming processes and to evaluate retrievals of ice water content (IWC), particle number concentration
538 N_t, and mean particle diameter D_m (e.g. Ryzhkov et al., 2018; Ryzhkov and Zrnic, 2019; Bukovčić et al., 2020; Carlin et al.
539 2021). The OLYMPEX mission took place on the Olympic Peninsula of Washington State (USA) from November 2015
540 through February 2016. University of North Dakota's (UND) Cessna Citation II equipped with an in-situ cloud payload
541 overpassed the National Science Foundation (NSF) Doppler On Wheels (DOW,- mobile polarimetric X-band radar with about
542 60 km range and 74 m radial resolution), placed in the Chehalis Valley at Lake Quinault (47.48° N, 123.86° W, 64 m altitude)
543 performing RHI scans within an azimuthal sector of 22 ~~°.~~ deg. Measurements and microphysical retrievals of the DOW and
544 the Citation, respectively, are currently evaluated and will then be compared at matched space-time coordinates for several
545 flight transects.

546

547 **4.2.2 Climate simulations with ICON-GCM**

548 A major part of the uncertainties in representing clouds and precipitation in atmospheric models can be attributed to unresolved
549 variability that affects resolved variables via non-linear processes. Current climate model horizontal resolutions are on the
550 order of 100 km. But even for NWP models, which have resolutions between 10 km for global and 1 km for regional
551 simulations, most cloud processes remain unresolved. The project ***Climate model PArameterizations informed by RAdar***
552 ***(PARA)*** evaluates and improves the representation of cloud and precipitation processes in particular for climate models and
553 focuses on precipitation formation in ice clouds. Since most surface precipitation over continents and extra-tropical oceans
554 involve the ice phase (Mülmenstädt et al., 2015; Field and Heymsfield, 2015) its reliable representation is paramount and thus
555 the focus of ***PARA***. Microphysical parameterizations typically consider only the mean cloud liquid or ice water content to
556 compute process rates, which causes biases in all nonlinear processes including radiation (e.g., Cahalan, 1994; Carlin et al.,

557 2002) and precipitation formation (e.g., Pincus and Klein, 2000). Realistic results thus require the tuning of process rates (e.g.,
558 Rotstayn, 2000) or realistic estimates of subgrid-scale cloud variability and its inclusion in the process parameterizations. To
559 tackle this issue, *PARA* exploits inherent model assumptions for treating fractional cloudiness. Since the early works of
560 Sommeria and Deardorff (1977), atmospheric models assume or predict some notion of subgrid-scale variability of relative
561 humidity. Some models do so by predicting cloud fraction (e.g., Tiedtke, 1993), others use a diagnostic representation of the
562 subgrid-scale probability density function (PDF) of total water specific humidity, q_t (e.g., Sundqvist et al., 1989; Smith, 1990;
563 Le Treut and Li, 1991; Rosch et al., 2015). Another option is to utilize a prognostic probability density function (PDF) of q_t
564 by assuming a functional form and predicting the shape parameters of the PDF (e.g., Tompkins, 2002; Neggers, 2009). The
565 German climate and weather prediction model ICON in its version dedicated to climate simulations (general circulation model
566 version; ICON-GCM) inherits the representation of physical processes from its predecessor ECHAM6 (Stevens et al., 2013)
567 and uses the Sundqvist et al. (1989) parameterization for a diagnostic PDF of the total-water specific humidity, q_t.

568 As a first step, *PARA* analyses the implied PDF of cloud ice using satellite observations from combined CloudSat-CALIPSO
569 radar-lidar satellite observations (DARDAR, Delanoë et al., 2014). Interestingly, a first direct comparison of IWC profiles
570 obtained from DARDAR with polarimetric retrievals based on the ground-based BoXPol radar shows an overall good
571 agreement, except for columns with an integrated ice water path IWP > 1 kg m^{-2}. In these regions pronounced polarimetric
572 signatures result in high IWC at higher altitudes, which are neither reproduced by reflectivity-only retrievals nor by the
573 DARDAR retrievals. The statistics are currently evaluated on a larger database, which is also used to investigate the impact
574 on the parameterizations in ICON-GCM. In the second step, a stochastic parameterization approach is taken to allow for an
575 unbiased computation of cloud microphysical process rates on average. Based on the cumulative distribution function (CDF),
576 a random number generator draws from the CDF according to the simulated likelihood a plausible value of the specific ice
577 mass based on which the microphysical process is computed. This specifically considers the formation of solid precipitation
578 (snow) from ice clouds via aggregation and accretion processes (Lohmann and Roeckner, 1996; Stevens et al., 2013), and
579 subsequently the evaporation of precipitation below the clouds. The result of the revised aggregation parameterization is
580 shown in Fig. 9. The increased aggregation rate, which is a linear function of the specific cloud ice, q_i, leads to an average
581 decrease in q_i. The aggregation rate is directly linked to the accretion rate, which lowers the effect of q_i decrease. An
582 investigation of the influence of the revised aggregation parameterization on the different microphysical process rates - which
583 are related to the ice phase - is currently performed. A detailed evaluation of the new versus old parameterization with the
584 ground-based polarimetric radar is on its way, and will in particular focus on the time scales of evaporation of precipitation
585 below the cloud.

4.2.3 Data assimilation

587 Within an idealized framework, Jung et al. (2008, 2010) and Zhu et al. (2020) demonstrated benefits of assimilating simulated
588 polarimetric data for the estimation of microphysical state variables. Up to now, however, direct assimilation of real

589   polarimetric data poses great challenges due to the deficiencies of cloud and precipitation schemes in NWP models in
590   realistically representing and providing the necessary information (optimally the distribution of particle size, shape and
591   orientations in all model grid boxes) required by a polarimetric radar observation operator and therefore causing large
592   representation error (Janjic et al., 2018). Both the specification of model error to examine uncertainty in microphysics (Feng
593   et al., 2021) and the specification of the observation error for polarimetric radar observations that include estimates of the
594   representation error (Zeng et al., 2021b), are investigated in the PROM-project **REDPOL**. For the assimilation of radar
595   reflectivity with an ensemble Kalman filter, several approaches for including model errors during data assimilation are
596   explored, including 1) additive noise with samples representing large-scale uncertainty (see Zeng et al., 2018), 2) combination
597   of large scale and unresolved scale uncertainty (Zeng et al., 2019), and finally 3) adding to these warm bubble triggering of
598   convective storms in case they are missing in the one hour forecast but present in corresponding observations (Zeng et al.,
599   2020). Applying Pol-EMVORADO to the analysis obtained by assimilating radar reflectivity from the German C-bBand
600   network), Fig. 6 illustrates the resulting differences of these three techniques in Z_{DR}-space. Obviously, synthetic Z_{DR} values
601   depend on the strategy used to specify the model error, putting another weight to the argument that assimilation of radar
602   reflectivity alone is not sufficient to constrain the estimation of microphysical state variables, and that polarimetric information
603   is required in addition. First results in this direction were reported by Putnam et al. (2019), who assimilated Z_{DR} below the
604   melting layer but reported problems in with the assimilation of K_{DP} data for a supercell case due to high observation errors as
605   a result of contamination from wet hail, dust and debris and- nonuniform beam filling.
606   .

607 **5 Summary and Perspectives**

608   The Priority Programme ***Polarimetric Radar Observations meet Atmospheric Modelling (PROM)*** (SPP 2115,
609   https://www2.meteo.uni-bonn.de/spp2115/) was established in April 2017 by the Senate of the Deutsche
610   Forschungsgemeinschaft (DFG, German Research Foundation) and is designed to run for six years. PROM is a coordinated
611   effort to foster partnerships between cloud modelers and radar meteorologists and thus to accelerate the exploitation of
612   polarimetric weather radars to improve the representation of cloud and precipitation processes in numerical models. The first
613   funding phase engaged in an as-complete-as-possible exploitation and understanding of nation-wide polarimetric
614   measurements complemented by state-of-the-art measurement devices and techniques available at supersites. Bulk
615   polarimetric measurements available over Germany are complemented with multi-frequency observations and spectral
616   polarimetry for detailed studies of ice and cloud microphysics. Thus, modellers now hold an unprecedented amount of three-
617   dimensional microphysics-related observational data in their hands to improve parameterizations. Key tools for the fusion of
618   radar polarimetry and atmospheric modelling, e.g. the Monte-Carlo Lagrangian particle model McSnow and the polarimetric
619   observation operator Pol-EMVORADO, have been developed. PROM started with detailed investigations of the representation
620   of cloud and precipitation processes in the COSMO and ICON atmospheric models exploiting polarimetric observation

621 operators. First improvements of the 2-moment cloud- and precipitation microphysics scheme are made and more are expected
622 in phase 2. ~~Also~~In addition, intercomparisons of microphysics schemes in radar space have been performed. Phase 1 further
623 developed microphysical retrievals, determined their uncertainties and started their exploitation for model evaluation and
624 radar-informed parameterizations. The developed prerequisites pave the way to finally exploit polarimetry for indirect and
625 direct data assimilation in the upcoming second funding phase.

626 Some tools developed in ~~p~~Phase 1, however, still require refinement in ~~p~~Phase 2. The T-matrix calculations for
627 electromagnetic scattering by spheroidal particles represent only a crude approximation to frozen and mixed-phase
628 hydrometeors, especially for pristine ice particles and aggregate snowflakes at cloud radar wavelengths. It is not possible to
629 reproduce observed polarimetric signatures of snow with the T-Matrix approach (i.e. homogeneous ice-air spheroids) and
630 realistic microphysics (shape, orientation). Refinements include interfacing to a new discrete dipole approximation (DDA)-
631 based scattering data base for realistic ice and snow particles for all relevant weather radar wavelengths and improvements of
632 the melting scheme of graupel and hail.

633 Based on the progress made, the fusion of radar polarimetry and atmospheric modelling can be approached even more
634 aggressively in ~~p~~Phase 2. While objective 1 received most attention in ~~p~~Phase 1, more projects will exploit the observational
635 insights and tools developed to finally improve parameterizations and assimilate polarimetric information, i.e. more emphasis
636 will be put on ~~Objectives~~ objectives 2 and 4 in ~~p~~Phase 2. Direct assimilation of polarimetric variables remains challenging,
637 because NWP models need to realistically represent and provide the necessary information required by a polarimetric radar
638 observation operator; ideally the distribution of particle size, shape and orientation would be required in all model grid boxes.
639 Indirect assimilation of polarimetric information (e.g. microphysical retrievals, and process signatures), however, is less
640 demanding to the model and should be pursued in parallel. Modern Bayesian data assimilation techniques are sensitive to both
641 model- and observation operator biases, so that further work on these issues is of great importance for a successful data
642 assimilation.

643

644 **Data availability**
645 The data presented in this paper are available through the authors upon request. Polarimetric radar data from the operational
646 C-band radar network is also available from the German Weather Service (DWD). Specific campaign data will be published
647 in addition.

648

649 **Author contributions**
650 Silke Trömel had the initial idea and mainly organized and structured the joint publication. Silke Trömel, Johannes Quaas, and
651 Clemens Simmer formed the editorial team consolidating the text. All authors contributed to specific sections of the paper and
652 commented on the paper.

653

Competing interests

Johannes Quaas is editor of ACP. The authors declare to have no additional conflict of interest.

Special issue statement

This article is the overview article of the ACP/AMT/GMD inter-journal special issue "Fusion of radar polarimetry and numerical atmospheric modelling towards an improved understanding of cloud and precipitation processes". It is not associated with a conference.

Acknowledgments

We gratefully acknowledge the funding of the German Research Foundation (DFG) to initialize the special priority program on the Fusion of Radar Polarimetry and Atmospheric Modelling (SPP-2115, PROM). The work of contributing authors was carried out in the framework of the projects Operation Hydrometeors (Grants TR 1023/16-1 and BL 945/2-1), IcePolCKa (HA 3314/9-1 and ZI 1132/5-1), ILACPR (Grant SH 1326/1-1), IMPRINT (Grant KN 1112/3-1), POLICE (Grants TR 1023/13-1 and VO 1504/5-1), PARA (Grants QU 311/21-1 and TR 1023/15-1), HydroColumn (Grant FR 4119/1-1), REDPOL (Grant JA 1077/5-1), and PICNICC (Grants KA 4162/2-1 and SE 2464/1-1). ILACPR gratefully acknowledges the computing time (project HBN33) granted by the John von Neumann Institute for Computing (NIC) and provided on the supercomputer JUWELS at Jülich Supercomputing Centre (JSC).

References

Alfieria, L., Thielen, J., and Pappenberger, J.: Ensemble hydro-meteorological simulation for flash flood early detection in southern Switzerland, J. Hydrol., 424, 143-153, doi:10.1016/j.jhydrol.2011.12.038, 2012.

Bauer, P., Thorpe, A., and Brunet, G.: The quiet revolution of numerical weather prediction, Nature 525, 47–55, doi:10.1038/nature14956, 2015.

Besic, N., Gehring, J., Praz, C., Figueras i Ventura, J., Grazioli, J., Gabella, M., Germann, U., and Berne, A.: Unraveling hydrometeor mixtures in polarimetric radar measurements, Atmos. Meas. Tech., 11, 4847–4866, doi:10.5194/amt-11-4847-2018, 2018.

Besic, N., Figueras i Ventura, J., Grazioli, J., Gabella, M., Germann, U., and Berne, A.: Hydrometeor classification through statistical clustering of polarimetric radar measurements: A semisupervised approach. Atmos. Meas. Tech., 9(9), 4425-4445, 2016

684

685 Bick, T., Simmer, C., Trömel, S., Wapler, K., Stephan, K., Blahak, U., Zeng, Y., and Potthast, R.: Assimilation of 3D-radar
686 Reflectivities with an Ensemble Kalman Filter on the Convective Scale, Quart. J. Roy. Meteor. Soc., 142, 1490–1504, 2016.
687

688 Blahak, U.: RADAR_MIE_LM and RADAR_MIELIB - Calculation of Radar Reflectivity from Model Output, COSMO
689 Technical Report No. 28, Consortium for Small Scale Modeling (COSMO), available online http://www.cosmo-
690 model.org/content/model/documentation/techReports/docs/techReport28.pdf, 2016.
691

692 Blahak, U. and De Lozar, A.: EMVORADO - Efficient Modular VOlume scan RADar Operator. A User's Guide, Deutscher
693 Wetterdienst, available online http://www.cosmo-model.org/content/model/documentation/core/emvorado_userguide.pdf,
694 2020.
695

696 Brdar, S. and Seifert, A.: McSnow: A Monte-Carlo Particle Model for Riming and Aggregation of Ice Particles in a
697 Multidimensional Microphysical Phase Space, J. Adv. Model. Earth Syst., 10(1), 187–206, doi:10.1002/2017MS001167, 2018.
698

699

700 Bukovčić, P., Ryzhkov, A., and Zrnić, D.: Polarimetric Relations for Snow Estimation—Radar Verification, Journal of Applied
701 Meteorology and Climatology, 59(5), 991-1009, doi:10.1175/JAMC-D-19-0140.1, 2020
702

703 Bühl, J., Seifert, P., Wandinger, U., Baars, H., Kanitz, T., Schmidt, J., Myagkov, A., Engelmann, R., Skupin, A., Heese, B.,
704 Klepel, A., Althausen, D., and Ansmann, A.: LACROS: The Leipzig Aerosol and Cloud Remote Observations System, in:
705 SPIE Remote Sensing, edited by Comeron, A., Kassianov, E. I., Schäfer, K., Stein, K., and Gonglewski, J. D., p. 889002,
706 Dresden, Germany, doi:10.1117/12.2030911, 2013.
707

708 Bühl, J., Seifert, P., Maygkov, A., and Ansmann, A.. Measuring ice- and liquid-water properties in mixed-phase cloud layers
709 at the Leipzig Cloudnet station, Atmos. Chem. Phys., 16, 10609-10620, doi: 10.5194/acp-16-10609-2016, 2016
710

711 Cahalan, R. F.: Bounded cascade clouds: albedo and effective thickness, Nonlinear Proc. In Geophysics., 1, 156-167, 1994.
712

713 Carlin, B., et al.: High-cloud horizontal inhomogeneity and solar albedo bias, J. Climate, 15, 2321 – 2339, 2002.
714

715 Carlin, J. T., Ryzhkov, A. V., Snyder, J. C., and Khain, A.: Hydrometeor Mixing Ratio Retrievals for Storm-Scale Radar Data
716 Assimilation: Utility of Current Relations and Potential Benefits of Polarimetry, Mon. Weather Rev. 144(8), 2981-3001,
717 doi:10.1175/MWR-D-15-461 0423.1., 2016.

718

Carlin, J. T., Reeves, H. D., and Ryzhkov, A. V.: Polarimetric Observations and Simulations of Sublimating Snow: Implications for Nowcasting. J. Appl. Meteor. Climatol., 60(8), 1035-1054, doi:10.1175/JAMC-D-21-0038.1, 2021.

Costa-Surós, M., Sourdeval, O., Acquistapace, C., Baars, H., Carbajal Henken, C., Genz, C., Hesemann, J., Jimenez, C., König, M., Kretzschmar, J., Madenach, N., Meyer, C. I., Schrödner, R., Seifert, P., Senf, F., Brueck, M., Cioni, G., Engels, J. F., Fieg, K., Gorges, K., Heinze, R., Siligam, P. K., Burkhardt, U., Crewell, S., Hoose, C., Seifert, A., Tegen, I., and Quaas, J.: Detection and attribution of aerosol–cloud interactions in large-domain large-eddy simulations with the ICOsahedral Non-hydrostatic model, Atmos. Chem. Phys., 20, 5657–5678, doi:10.5194/acp-20-5657-2020, 2020.

Delanoë, J., Heymsfield, A. J., Protat, A., Bansemer, A., and Hogan, R. J.: Normalized particle size distribution for remote sensing application, J. Geophys. Res. Atmos., 119, 4204-4227, doi:10.1002/2013JD020700, 2014.

Diederich, M., Ryzhkov, A., Simmer, C., Zhang, P., and Trömel, S.: Use of specific attenuation for rainfall measurement at X-band radar wavelengths - Part 1: Radar calibration and partial beam blockage estimation, J. Hydrometeor., 16, 2, 487-502, doi: 10.1175/JHM-D-14-0066.1, 2015a.

Diederich, M., Ryzhkov, A., Simmer, C., Zhang, P., and Trömel, S.: Use of specific attenuation for rainfall measurement at X-band radar wavelengths - Part 2: Rainfall estimates and comparison with rain gauges, J. Hydrometeor., 16, 2, 503-516, doi: 10.1175/JHM-D-14-0067.1, 2015b.

Dipankar, A., Stevens, B., Heinze, R., Moseley, C., Zängl, G., Giorgetta, M., and Brdar, S.: Large eddy simulations using the general circulation model ICON, J. Adv. Model. Earth Sy., 7, 963–986, doi.org/10.1002/2015MS000431, 2015.

Feng, Y., T. Janjic, Y. Zeng, A.Seifert, J. Min, 2021, Representing microphysical uncertainty in convective-scale data assimilation using additive noise, J. Adv. Model. Earth Sy., 2021 (submitted).

Field, P. R. and Heymsfield, A. J.: Importance of snow to global precipitation, Geophys. Res. Lett., 42, 9512–9520, doi:10.1002/2015GL065497, 2015.

Field, P. R., Lawson, R. P., Brown, P. R. A., Lloyd, G., Westbrook, C., Moisseev, D., Miltenberger, A., Nenes, A., Blyth, A., Choularton, T., Connolly, P., Buehl, J., Crosier, J., Cui, Z., Dearden, C., DeMott, P., Flossmann, A., Heymsfield, A., Huang, Y., Kalesse, H., Kanji, Z. A., Korolev, A., Kirchgaessner, A., Lasher-Trapp, S., Leisner, T., McFarquhar, G., Phillips, V.,

Stith, J., and Sullivan, S.: Secondary Ice Production: Current State of the Science and Recommendations for the Future, Meteorological Monographs, 58, 7.1-7.20, doi: 10.1175/AMSMONOGRAPHS-D-16-0014.1, 2017

Forster, P., Storelvmo, T., Armour, K., Collins, W., Dufresne, J. L., Frame, D., Lunt, D. J., Mauritsen, T., Palmer, M. D., Watanabe, M., Wild, M., and Zhang, H.: The Earth's Energy Budget, Climate Feedbacks, and Climate Sensitivity. In: Climate Change 2021: The Physical Science Basis. Contribution of Working Group I to the Sixth Assessment Report of the Intergovernmental Panel on Climate Change, Cambridge University Press, in press, 2021.

Frech, M., and Hubbert, J.: Monitoring the differential reflectivity and receiver calibration of the German polarimetric weather radar network, Atmos. Meas. Tech., 13, 1051–1069, doi: 10.5194/amt-13-1051-2020, 2020.

Gao, W., Sui, C.-H., Chen Wang, T.-C. and Chang, W.-Y.: An evaluation and improvement of microphysical parameterization from a two-moment cloud microphysics scheme and the Southwest Monsoon Experiment (SoWMEX)/Terrain-influenced Monsoon Rainfall Experiment (TiMREX) observations, J. Geophys. Res. Atmos., 116, 1-13, doi:10.1029/2011JD015718, 2011.

Gasper, F., Görgen, K., Shrestha, P., Sulis, M., Rihani, J., Geimer, M., and Kollet, S.: Implementation and scaling of the fully coupled Terrestrial Systems Modeling Platform (TerrSysMP v1. 0) in a massively parallel supercomputing environment–a case study on JUQUEEN (IBM Blue Gene/Q), Geosci. Model Dev., 7(5), 2531-2543, 2014.

Gehring, J., Oertel, A., Vignon, E., Jullien, N., Besic, N., and Berne, A.: Microphysics and dynamics of snowfall associated with a warm conveyor belt over Korea, Atmos. Chem. Phys., 20, 7373–7392, doi: 10.5194/acp-20-7373-2020, 2020.

Grazioli, J., Tuia, D., and Berne, A.: Hydrometeor classification from polarimetric radar measurements: a clustering approach, Atmos. Meas. Tech., 8(1), 149-170, 2015.

Flamant, C., Knippertz, P., Fink, A.H., Akpo, A., Brooks, B., Chiu, C.J., Coe, H., Danuor, S., Evans, M., Jegede, O., Kalthoff, N., Konaré, A., Liousse, C., Lohou, F., Mari, C., Schlager, H., Schwarzenboeck, A., Adler, B., Amekudzi, L., Aryee, J., Ayoola, M., Batenburg, A.M., Bessardon, G., Borrmann, S., Brito, J., Bower, K., Burnet, F., Catoire, V., Colomb, A., Denjean, C., Fosu-Amankwah, K., Hill, P.G., Lee, J., Lothon, M., Maranan, M., Marsham, J., Meynadier, R., Ngamini, J., Rosenberg, P., Sauer, D., Smith, V., Stratmann, G., Taylor, J.W., Voigt, C., and Yoboué, V.: The Dynamics–Aerosol–Chemistry–Cloud Interactions in West Africa Field Campaign: Overview and Research Highlights, B. Am. Meteorol. Soc., 99, 83–104,doi:10.1175/BAMS-D-16-0256.1, 2018

784 Fridlind, A. M., van Lier-Walqui, M., Collis, S., Giangrande, S. E., Jackson, R. C., Li, X., Matsui, T., Orville, R., Picel, M.
785 H., Rosenfeld, D., Ryzhkov, A., Weitz, R., and Zhang, P.: Use of polarimetric radar measurements to constrain simulated
786 convective cell evolution: a pilot study with Lagrangian tracking, Atmos. Meas. Tech., 12, 2979–3000, doi:10.5194/amt-12-
787 2979-2019, 2019.

788

789 Hashino, T., and Tripoli, G. J.: The Spectral Ice Habit Prediction System (SHIPS). Part I: Model Description and Simulation
790 of the Vapor Deposition Process, J. Atmos. Sci., 64(7), 2210-2237, doi:10.1175/JAS3963.1, 2007.

791

792 Heinze, R., Dipankar, A., Henken, C. C., Moseley, C., Sourdeval, O., Trömel, S., Xie, X., Adamidis, P., Ament, F., Baars, H.
793 Barthlott, C., Behrendt, A., Blahak, U. , Bley, S. , Brdar, S., Brueck, M., Crewell, S., Deneke, H., Girolamo, P. D., Evaristo,
794 R., Fischer, J., Frank, C., Friederichs, P., Göcke, T., Gorges, K., Hande, L., Hanke, M., Hansen, A., Hege, H.-C., Hoose, C.,
795 Jahns, T., Kalthoff, N., Klocke, D., Kneifel, S., Knippertz, P., Kuhn, A., Laar, T., Macke, A., Maurer, V., Mayer, B., Meyer,
796 C. I., Muppa, S. K., Neggers, R. A. J., Orlandi, E., Pantillon, F. , Pospichal, B., Röber, N., Scheck, L., Seifert, A., Seifert, P.,
797 Senf, F. , Siligam, P., Simmer, C., Steinke, S., Stevens, B., Wapler, K., Weniger, M., Wulfmeyer, V., Zängl, G., Zhang, D.,
798 and Quaas, J.: Large-eddy simulations over Germany using ICON: A comprehensive evaluation, Q. J. Roy. Meteor. Soc., 143,
799 69-100, doi:10.1002/qj.2947, 2017.

800

801 Heymsfield, A., Bansemer, A., Wood, N. B., Liu, G., Tanelli, S., Sy, O. O., Poellot, M., and Liu, C.: Toward Improving Ice
802 Water Content and Snow-Rate Retrievals from Radars. Part II: Results from Three Wavelength Radar–Collocated In Situ
803 Measurements and CloudSat–GPM–TRMM Radar Data, J. Appl. Meteor. Climatol., 57(2), 365-389. Retrieved Apr 6, 2021,
804 from https://journals.ametsoc.org/view/journals/apme/57/2/jamc-d-17-0164.1.xml, 2018.

805

806 Hogan, R. J., Tian, L., Brown, P. R. A., Westbrook, C. D., Heymsfield, A. J., and Eastment, J. D.: Radar Scattering from Ice
807 Aggregates Using the Horizontally Aligned Oblate Spheroid Approximation, J. Appl. Meteor. Climatol., 51(3), 655-671,
808 doi:10.1175/JAMC-D-11-074.1, 2012.

809

810 Ilotoviz, E., Khain, A., Ryzhkov, A. V., and Snyder, J. C.: Relation between Aerosols, Hail Microphysics, and ZDR Columns,
811 J. Atmos. Sci., 75, 1755-1781, doi:10.1175/JAS-D-17-0127.1, 2018.

812

813 Janjic, T., Bormann, N., Bocquet, M., Carton, J. A., Cohn, S. E., Dance, S. L., Losa, S. N., Nichols, N. K., Potthast, R., Waller,
814 J. A., and Weston, P.: On the representation error in data assimilation, Q. J. R. Meteorol. Soc., 144:713, 1257-1278, 2018.

815

816 Jung, Y., Xue, M., Zhang, G., and Straka, J.: Assimilation of simulated polarimetric radar data for a convective storm using
817 ensemble Kalman filter. Part II: Impact of polarimetric data on storm analysis, Mon. Wea. Rev., 136, 2246–2260,
818 doi:10.1175/2007MWR2288.1, 2008.

819

820 Jung, Y., Xue, M., and Zhang, G.: Simultaneous Estimation of Microphysical Parameters and the Atmospheric State Using
821 Simulated Polarimetric Radar Data and an Ensemble Kalman Filter in the Presence of an Observation Operator Error, Mon.
822 Wea. Rev., 138, 539–562, doi:10.1175/2009MWR2748.1, 2010.

823

824 Jung, Y., Xue, M., and Tong, M.: Ensemble Kalman Filter Analyses of the 29—30 May 2004 Oklahoma Tornadic
825 Thunderstorm Using One- and Two-Moment Bulk Microphysics Schemes, with Verification against Polarimetric Radar Data,
826 Mon. Wea. Rev., 140, 1457-1475, doi: MWR-D-11-00032.1, 2012

827

828 Kalesse, H., Szyrmer, W., Kneifel, S., Kollias, P., and Luke, E.: Fingerprints of a riming event on cloud radar Doppler spectra:
829 observations and modeling, Atmos. Chem. Phys., 16, 2997–3012, doi: 10.5194/acp-16-2997-2016, 2016.

830

831 Khain, A., Rosenfeld, D., and Pokrovsky, A.: Aerosol impact on the dynamics and microphysics of convective clouds, Q. J.
832 R. Meteorol. Soc., 131, 2639–2663, doi:10.1256/qj.04.62, 2005.

833

834 Khain, A. P., Beheng, K. D., Heymsfield, A., Korolev, A., Krichak, S. O., Levin, Z., Pinsky, M., Phillips, V., Prabhakaran, T.,
835 Teller, A., et al.: Representation of microphysical processes in cloud-resolving models: Spectral (bin) microphysics versus
836 bulk parameterization, Rev. Geophys., 53, 247– 322, doi:10.1002/2014RG000468, 2015.

837

838 Kleine, J., Voigt, C., Sauer, D., Schlager, H., Scheibe, M., Kaufmann, S. , Jurkat-Witschas, T., Kärcher, B., and Anderson B.:
839 In situ observations of ice particle losses in a young persistent contrail, Geophs. Res. Lett., doi:10.1029/2018GL079390, 2018.

840

841 Kneifel S., A. von Lerber, J. Tiira, D. Moisseev, P. Kollias, and J. Leinonen: Observed Relations between Snowfall
842 Microphysics and Triple-frequency Radar Measurements, J. Geophys. Res., 120, 6034-6055, doi: 10.1002/2015JD023156,
843 2015.

844

845 Kneifel, S., and Moisseev, D.: Long-term statistics of riming in non-convective clouds derived from ground-based Doppler
846 cloud radar observations, J. Atmos. Sci., 77, 3495–3508, doi: 10.1175/JAS-D-20-0007.1, 2020.

847

848 Kollias, P., Albrecht, B.A., and Marks Jr F.: Why Mie?Accurate observations of vertical air velocities and raindrops using a
849 cloud radar. Bulletin of the American Meteorological Society, 83(10),. 1471-1484, doi: 10.1175/BAMS-83-10-1471 2002

850

851 Kumjian, M.R.: Principles and applications of dual-püolarization wheather radar. Part I: Description of the polarimetric radar
852 variables. J. Operational Meteor., 1(19), 226-242, doi: 10.15191/nwajom.2013.0119, 2013

853

854 Kumjian, M. R.: The impact of precipitation physical processes on the polarimetric radar variables, Dissertation, University
855 of Oklahoma, Norman Campus, https://hdl.handle.net/11244/319188, 2012

856

857 Kumjian, M. R., Khain, A. P., Benmoshe, N., Ilotoviz, E., Ryzhkov, A. V., and Phillips, V. T. J.: The anatomy and physics of
858 Z_{DR} columns: Investigating a polarimetric radar signature with a spectral bin microphysical model, J. Appl. Meteor. Climatol.,
859 53, 1820-1843, 2014.

860

861 Kumjian, M. R., Tobin, D. M., Oue, M., and Kollias, P.: Microphysical insights into ice pellet formation revealed by fully
862 polarimetric Ka-band Doppler radar, J. Appl. Meteor. Climatol., 59, 1557–1580, doi: 10.1175/JAMC-D-20-0054.1, 2020.

863

864 Kuster, C. M., Schuur, T. J., Lindley, T. T., and Snyder, J. C.: Using ZDR Columns in Forecaster Conceptual Models and
865 Warning Decision-Making, Weather and Forecasting, 35(6), 2507-2522, 2020.

866

867 Le Treut, H. and Li, Z.-X.: Sensitivity of an atmospheric general circulation model to prescribed SST changes: Feedback
868 effects associated with the simulation of cloud optical properties, Clim. Dyn., 5, 175–187, 1991.

869

870 Li, H., and Moisseev, D.: Two layers of melting ice particles within a single radar bright band: interpretation and implications,
871 Geophys. Res. Lett., 47, e2020GL087499, doi: 10.1029/2020GL087499, 2020.

872

873 Libbrecht, K. G.: The physics of snow crystals, Rep. Prog. Phys., 68, 855–895, doi:10.1088/0034-4885/68/4/R03, 2005.

874

875 Lohmann U. und E. Roeckner, Design and performance of a new cloud microphysics scheme developed for the ECHAM
876 general circulation model, Clim. Dyn., 12, 557-572, 1996.

877

878 Lukach, M., Dufton, D., Crosier, J., Hampton, J.M., Bennett, L. and Neely III, R.R.. Hydrometeor classification of quasi-
879 vertical profiles of polarimetric radar measurements using a top-down iterative hierarchical clustering method. Atmos. Meas.
880 Tech, 14(2), pp.1075-1098, 2021

881

882 Luke E.P., Yang, F., Kollias, P., Vogelmann, A.M., Maahn, M.: New insights into ice multiplication using remote-sensing
883 observations of slightly supercooled mixed-phase clouds in the Arctic. PNAS, 118(13), e2021387118,
884 doi:10.1073/pnas.2021387118, 2021

885 Matrosov, S. Y., Reinking, R. F., Kropfli, R. A., Martner, B. E., and Bartram, B. W. (2001), On the use of radar depolarization
886 ratios for estimating shapes of ice hydrometeors in winter clouds, Journal of Applied Meteorology, 40, 479-490,
887 doi:10.1175/1520-0450(2001)040h0479:OTUORDi2.0.CO;2.

888

889 Matsui, T., Dolan, B., Rutledge, S. A., Tao, W.-K., Iguchi, T., Barnum, J., and Lang, S. E.: POLARRIS: A POLArimetric
890 Radar Retrieval and Instrument Simulator, J. Geophys. Res.-Atmos., 124, 4634–4657, doi:10.1029/2018JD028317, 2019.

891

892 Mellado, J.P., Stevens, B., Schmidt, H., and Peters, N.: Buoyancy reversal in cloud-top mixing layers, Q.J.R. Meteorol. Soc.,
893 135: 963-978., doi:10.1002/qj.417, 2009.

894

895 Mendrok, J., Blahak, U., Snyder, J. C., and Carlin, J. T.: The polarimetric efficient modular volume scan radar forward operator
896 Pol-EMVORADO, Geosci. Model Dev., 2021 (in preparation for this Special Issue).

897

898 Mishchenko, M. I.: Calculation of the amplitude matrix for a nonspherical particle in a fixed orientation, Appl. Opt. 39, 1026-
899 1031, 2000.

900

901 Moisseev, D. N., Lautaportti, S., Tyynela, J., and Lim, S.: Dualpolarization radar signatures in snowstorms: Role of snowflake
902 aggregation, J. Geophys. Res. Atmos., 120, 12 644–12 655, doi:10.1002/2015JD023884, 2015.

903

904 Morrison, H. and Milbrandt, J. A.: Parameterization of Cloud Microphysics Based on the Prediction of Bulk Ice Particle
905 Properties. Part I: Scheme Description and Idealized Tests, J. Atmos. Sci., 72(1), 287-311, 2015.

906

907 Morrison, H., van Lier-Walqui, M., Fridlind, A. M., Grabowski, W. W., Harrington, J. Y., and Hoose, C., et al.: Confronting
908 the challenge of modeling cloud and precipitation microphysics. Journal of Advances in Modeling Earth Systems, 12,
909 e2019MS001689. doi:10.1029/2019MS001689, 2020.

910

911 Mülmenstädt, J., Sourdeval, O., Delanoë, J., and Quaas, J.: Frequency of occurrence of rain from liquid-, mixed- and ice-phase
912 clouds derived from A-Train satellite retrievals, Geophys. Res. Lett., 42, 6502-6509, doi:10.1002/2015GL064604, 2015.

913 Murphy, A. M., Ryzhkov, A., & Zhang, P.: Columnar vertical profile (CVP) methodology for validating polarimetric radar
914 retrievals in ice using in situ aircraft measurements. J. Atmos. Oceanic Technol., 37(9), 1623-1642, doi:10.1175/JTECH-D-
915 20-0011.1, 2020.

917 Myagkov, A., Seifert, P., Bauer-Pfundstein, M., and Wandinger, U.: Cloud radar with hybrid mode towards estimation of
918 shape and orientation of ice crystals, Atmos. Meas. Tech., 9, 469–489, doi:10.5194/amt-9-469-2016, 2016.

920 Neggers, R. A.: A dual mass flux framework for boundary layer convection. Part II: Clouds, J. Atmos. Sci., 66, 1489–1506,
921 doi:10.1175/2008JAS2636.1, 2009.

923 Neto, J. D., Kneifel, S., Ori, D., Trömel, S., Handwerker, J., Bohn, B., Hermes, N., Mühlbauer, K., Lenefer, M., and Simmer,
924 C.: The TRIple-frequency and Polarimetric radar Experiment for improving process observation of winter precipitation. Earth
925 Syst. Sci. Data, 11, 845–863, doi: 10.5194/essd-11-845-2019, 2019.

927 Nguyen, C., Wolde, M., Baibakov, K., and Korolev, A.: Detection and estimation of high ice water content using X- and W-
928 band dual-polarization airborne radar data, 38th Conf. on Radar Meteorology, Chicago, IL, Amer. Meteor. Soc., 89,
929 https://ams.confex.com/ams/38RADAR/webprogram/Paper321101.html, 2017.

931 Nguyen, C. M., Wolde, M., and Korolev, A.: Determination of ice water content (IWC) in tropical convective clouds from X-
932 band dual-polarization airborne radar, Atmos. Meas. Tech., 12, 5897–5911, doi: 10.5194/amt-12-5897-2019, 2019.

934 Ori, D., V. Schemann, M. Karrer, J. Dias Neto, L. von Terzi, A. Seifert, and S. Kneifel: Evaluation of ice particle growth in
935 ICON using statistics of multi-frequency Doppler cloud radar observations, Q. J. Roy. Meteor. Soc., 146: 3830– 3849.
936 doi:10.1002/qj.3875, 2020

937 Oue, M., A. Tatarevic, P. Kollias, D. Wang, K. Yu, and A.M. Vogelmann: The Cloud-resolving model Radar SIMulator (CR-
938 SIM) Version 3.3: description and applications of a~virtual observatory, Geoscientific Model Development, 13: 1975-1998.
939 doi: 10.5194/gmd-13-1975-2020, 2020.

940 Oue, M., Kollias, P., Ryzhkov, A., and Luke, E. P.: Toward exploring the synergy between cloud radar polarimetry and Doppler
941 spectral analysis in deep cold precipitating systems in the Arctic, J. Geophys. Res. Atmos., 123, 2797–2815, doi:
942 10.1002/2017JD027717, 2018.

943 Phillips, V. T. J., Yano, J., & Khain, A. (2017). Ice Multiplication by Breakup in Ice–Ice Collisions. Part I: Theoretical
944 Formulation, J. Atmos. Sci., *74*(6), 1705-1719

945 Pfitzenmayer L., Unal, C. M. H., Dufournet, Y., Ruschenberg, H. W. J.: Observing ice particle growth along fall streaks in
946 mixed-phase clouds using spectral polarimetric radar data, Atmos. Chem. Phys., 18, 7843-7863, doi: 10.5194/acp-18-7843-
947 2018, 2018.

948 Pincus, R. and Klein, S.: Unresolved spatial variability and microphysical process rates in large-scale models, J. Geophys.
949 Res., 105, 27059 - 27065, 2000.
950
951 Putnam, B., Xue, M., Jung, Y., Snook, N., and Zhang, G.: Ensemble Kalman Filter Assimilation of Polarimetric Radar
952 Observations for the 20 May 2013 Oklahoma Tornadic Supercell Case, Mon. Wea. Rev., 147, 2511–2533, doi:10.1175/MWR-
953 D-18-0251.1, 2019.
954
955 Radenz, M., Bühl, J., Seifert, P., Baars, H., Engelmann, R., Barja González, B., Mamouri, R.-E., Zamorano, F., and Ansmann,
956 A.: Hemispheric contrasts in ice formation in stratiform mixed-phase clouds: Disentangling the role of aerosol and dynamics
957 with ground-based remote sensing, Atmos. Chem. Phys. Discuss. [preprint], https://doi.org/10.5194/acp-2021-360, in review,
958 2021.
959
960 Reimann, L., Simmer, C., and Trömel, S.: Dual-polarimetric radar estimators of liquid water content over Germany, Accepted
961 for Meteorol. Z. (Contrib. Atm. Sci.), doi:10.1127/metz/2021/1072, 2021.
962
963 Ribaud, J.-F., L. A. T. Machado, and T. Biscaro: X-band dual-polarization radar-based hydrometeor classification for Brazilian
964 tropical precipitation systems, Atmos. Meas. Tech., 12, 811–837, doi.org/10.5194/amt-12-811-2019, 2019.
965
966 Rosch, J., et al.: Analysis of diagnostic climate model cloud parameterisations using large-eddy simulations, Q. J. R. Meteorol.
967 Soc., 141, 2199-2205, doi:10.1002/qj.2515, 2015.
968
969 Rotstayn, L. D.: On the tuning of autoconversion parameterizations in climate models, J. Geophys. Res., 105, 15,495–15,507,
970 2000.
971
972 Ryzhkov, A. V., Zrnic, D. S., and Gordon, B. A.: Polarimetric Method for Ice Water Content Determination, J. Appl. Meteor.
973 Climatol., 37, 125-134, 1998.
974

975 Ryzhkov, A., Pinsky, M., Pokrovsky, A., and Khain, A.: Polarimetric Radar Observation Operator for a Cloud Model with
976 Spectral Microphysics, J. Appl. Meteor. Climatol., 50, 873-894, 2011.
977
978 Ryzhkov, A., Zhang, P., Reeves, H., Kumjian, M., Tschallener, T., Trömel, S., and Simmer, C.: Quasi-vertical profiles – a
979 new way to look at polarimetric radar data, J. Atmos. Oceanic Technol., 33, 551-562, doi: 10.1175/JTECH-D-15-0020.1, 2016.
980
981 Ryzhkov, A., Bukovcic, P., Murphy, A., Zhang, P., and McFarquhar, G.: Ice Microphysical Retrievals Using Polarimetric
982 Radar Data. In Proceedings of the 10th European Conference on Radar in Meteorology and Hydrology, Ede, The Netherlands,
983 1–6 July 2018.
984
985 Ryzhkov, A. and Zrnic, D.: Radar Polarimetry for Weather Observations, Springer Atmospheric Sciences, 486 pp., 2019.
986
987 Schinagl, K., Friederichs, P., Trömel, S., and Simmer, C.: Gamma Drop Size Distribution Assumptions in Bulk Model
988 Parameterizations and Radar Polarimetry and Their Impact on Polarimetric Radar Moments, J. Appl. Meteor. Climatol., 58,
989 467–478, doi: 10.1175/JAMC-D-18-0178.1, 2019.
990
991 Schrom, R. S. and Kumjian, M. R.: Bulk-Density Representations of Branched Planar Ice Crystals: Errors in the Polarimetric
992 Radar Variables, J. Appl. Meteor. Climatol., 57(2), 333-346, 2018.
993
994 Seifert, A. and Beheng, K. D.: A two-moment cloud microphysics parameterization for mixed-phase clouds. Part 1: Model
995 description, Meteorol. Atmos. Phys., 92, 45-66, doi: 10.1007/s00703-005-0112-4, 2006.
996 Shrestha, P., Sulis, M., Masbou, M., Kollet, S. and Simmer, C: A scale-consistent Terrestrial System Modeling Platform based
997 on COSMO, CLM and ParFlow, Mon. Wea. Rev., 142, 3466-3483, doi: 10.1175/MWR-D-14-00029.1, 2014
998 Shrestha, P.: Clouds and vegetation modulate shallow groundwater table depth, 22, 753 – 763, doi:10.1175/JHM-D-20-0171.1,
999 2021
1000 Shrestha, P., Trömel, S., Evaristo, R., and Simmer, C.: Evaluation of modeled summertime convective storms using
1001 polarimetric radar observations, Atmos. Chem. Phys. Discuss. [preprint], https://doi.org/10.5194/acp-2021-404, in review,
1002 2021a.
1003 Shrestha, P., Mendrok, J., Pejcic, V., Trömel, S., and Blahak, U.: The impact of uncertainties in model microphysics, retrievals
1004 and forward operators on model evaluations in polarimetric radar space, Geosci. Model Dev., 2021b (submitted).
1005

1006 Shupe, M. D., Kollias, P., Matrosov, S. Y., and Schneider, T. L.: Deriving mixed-phase cloud properties from Doppler radar
1007 spectra, J. Atmos. Oceanic Technol., 21, 660–670, doi: 10.1175/1520-0426(2004)021<0660:DMCPFD>2.0.CO;2, 2004.
1008
1009 Simmel, M., Bühl, J., Ansmann, A., and Tegen, I.: Ice phase in altocumulus clouds over Leipzig: remote sensing observations
1010 and detailed modeling, Atmos. Chem. Phys., 15, 10453–10470, doi:10.5194/acp-15-10453-2015, 2015.
1011
1012 Simmer, C., Thiele-Eich, I., Masbou, M., Amelung, W., Crewell, S., Diekkrueger, B., Ewert, F., Hendricks Franssen, H.-J.,
1013 Huisman, A. J., Kemna, A., Klitzsch, N., Kollet, S., Langensiepen, M., Löhnert, U., Rahman, M., Rascher, U., Schneider, K.,
1014 Schween, J., Shao, Y., Shrestha, P., Stiebler, M., Sulis, M., Vanderborght, J., Vereecken, H., van der Kruk, J., Zerenner, T.,
1015 and Waldhoff, G.: Monitoring and Modeling the Terrestrial System from Pores to Catchments - the Transregional
1016 Collaborative Research Center on Patterns in the Soil-Vegetation-Atmosphere System, B. Am. Meteorol. Soc., 96, 1765–1787,
1017 doi: 10.1175/BAMS-D-13-00134.1, 2015.
1018
1019 Simmer, C., Adrian, G., Jones, S., Wirth, V., Goeber, M., Hohenegger, C., Janjic, T., Keller, J., Ohlwein, C., Seifert, A.,
1020 Trömel, S., Ulbrich, T., Wapler, K., Weissmann, M., Keller, J., Masbou, M., Meilinger, S., Riss, N., Schomburg, A., Vormann,
1021 A., and Weingaertner, C.: HErZ - The German Hans-Ertel Centre for Weather Research. B. Am. Meteorol. Soc., 1057-1068,
1022 doi: 10.1175/BAMS-D-13-00227.1, 2014
1023
1024 Smith, R. N.: A scheme for predicting layer clouds and their water content in a general circulation model, Q. J. R. Meteorol.
1025 Soc., 116, 435–460, doi:10.1002/qj.49711649210, 1990.
1026
1027 Snyder, J.C., Ryzhkov, A.V., Kumjian, M.R., Khain, A.P., and Picca, J.C.: A ZDR column detection algorithm to examine
1028 convective storm updrafts, Weather and Forecasting, 30, 1819-1844, 2015.
1029
1030 Sommeria, G. and Deardorff, J. W.: Subgrid-scale condensation models of non-precipitating clouds, J. Atmos. Sci., 34, 344-
1031 355, 1977.
1032
1033 Sourdeval, O., Gryspeerdt, E., Krämer, M., Goren, T., Delanoë, J., Afchine, A., Hemmer, F., and Quaas, J.: Ice crystal number
1034 concentration estimates from lidar–radar satellite remote sensing – Part 1: Method and evaluation, Atmos. Chem. Phys., 18,
1035 14327–14350, doi: 10.5194/acp-18-14327-2018, 2018.
1036
1037 Spek, A. L. J., Unal, C. M. H., Moisseev, C. N., Russchenberg, H. W. J., Chandrasekar, V., Dufournet, Y.: A New Techniques
1038 to Categorize and Retrieve the Microphysical Properties of Ice Particles above the Melting Layer Using Radar Dual-
1039 Polarization Spectral Analysis, Jtech,doi: 10.1175/2007JTECHA944.1, 2008.

1040

Stevens, B., Acquistapace, C., Hansen, A., Heinze, R., Klinger, C., Klocke, D., Schubotz, W., Windmiller, J., Adamidis, P., Arka, I., Barlakas, V., Biercamp, J., Brueck, M., Brune, S., Buehler, S., Burkhardt, U., Cioni, G., Costa-Surós, M., Crewell, S., Crueger, T., Deneke, H., Friederichs, P., Carbajal Henken, C., Hohenegger, C., Jacob, M., Jakub, F., Kalthoff, N., Köhler, M., Van Laar, T. W., Li, P., Löhnert, U., Macke, A., Madenach, N., Mayer, B., Nam, C., Naumann, A. K., Peters, K., Poll, S. , Quaas, J., Röber, N., Rochetin, N., Rybka, H., Scheck, L., Schemann, V., Schnitt, S., Seifert, A., Senf, F., Shapkalijevski, M., Simmer, C., Singh, S., Sourdeval, O., Spickermann, D., Strandgren, J., Tessiot, O., Vercauteren, N., Vial, J., Voigt, A., and Zängl, G.: Large-eddy and storm resolving models for climate prediction - the added value for clouds and precipitation, J. Meteorol. Soc. Japan, 98, doi:10.2151/jmsj. 2020-021, 2020.

Stevens, B., et al.: Atmospheric component of the MPI-M Earth System Model: ECHAM6, J. Adv. Model. Earth Syst. 5: 146–172, doi: 10.1002/jame.20015, 2013.

Stevens, B. and Feingold, G.: Untangling Aerosol Effects on Clouds and Precipitation in a Buffered System, Nature, 461, 607-613, 2009.

Sundqvist, H., et al., Condensation and cloud parameterization studies with a mesoscale numerical weather prediction model, Mon. Weather Rev., 117, 1641–1657, 1989.

Takahashi, T.: High ice crystal production in winter cumuli over the Japan Sea, Geophysical research letters, 20.6, 451-454, 1993.

Takahashi, T., Yoshihiro N., and Yuzuru K.: Possible high ice particle production during graupel–graupel collisions, J. Atmos. Sci., 52.24, 4523-4527, 1995.

Takahashi, T.: Influence of liquid water content and temperature on the form and growth of branched planar snow crystals in a cloud, J. Atmos. Sci., 71.11, 4127-4142, 2014.

Tiedtke, M.: Representation of clouds in large scale models, Mon. Weather Rev., 121, 3040–3061, 1993.

Tompkins, A.: A prognostic parameterization for the subgrid-scale variability of water vapor and clouds in large-scale models and its use to diagnose cloud cover, J. Atmos. Sci., 59:1917- 1942, 2002.

1072

1073   Trömel, S., Quaas, J., Crewell, S., Bott, A., and Simmer, C.: Polarimetric Radar Observations Meet Atmospheric Modelling.
1074   19th International Radar Symposium (IRS), Bonn, doi: 10.23919/IRS.2018.8448121, 2018.

1075

1076   Trömel, S., Ryzhkov, A. V., Hickman, B., Mühlbauer, K., and Simmer, C.: Polarimetric Radar Variables in the Layers of
1077   Melting and Dendritic Growth at X Band—Implications for a Nowcasting Strategy in Stratiform Rain, J. Appl. Meteor.
1078   Climatol., 58, 2497–2522, doi:10.1175/JAMC-D-19-0056.1, 2019.

1079

1080   Trömel, S., A. V. Ryzhkov, P. Zhang, and C. Simmer: The microphysical information of backscatter differential phase δ in the
1081   melting layer, J. Appl. Meteor. Climatol., 53, 2344-2359, 2014.

1082

1083   Verlinde, J., Rambukkange, M. P., Clothiaux, E. E., McFarquhar, G. M., and Eloranta, E. W.: Arctic multilayered, mixed-
1084   phase cloud processes revealed in millimeter-wave cloud radar Doppler spectra, J. Geophys. Res. Atmos., 118, 13199 –13213,
1085   doi: 10.1002/2013JD020183, 2013.

1086

1087   Vogl, T., Maahn, M., Kneifel, S., Schimmel, W., Moisseev, D., and Kalesse-Los, H.: Using artificial neural networks to predict
1088   riming from Doppler cloud radar observations, Atmos. Meas. Tech. Discuss. [preprint], https://doi.org/10.5194/amt-2021-137,
1089   in review, 2021.

1090

1091   Voigt, C., Schumann, U., Jurkat, T., Schäuble, D., Schlager, H., Petzold, A., Gayet, J.-F., Krämer, M., Schneider, J., Borrmann,
1092   S., Schmale, J., Jessberger, P., Hamburger, T., Lichtenstern, M., Scheibe, M., Gourbeyre, C., Meyer, J., Kübbeler, M., Frey,
1093   W., Kalesse, H., Butler, T., Lawrence, M. G., Holzäpfel, F., Arnold, F., Wendisch, M., Döpelheuer, A., Gottschaldt, K.,
1094   Baumann, R., Zöger, M., Sölch, I., Rautenhaus, M., and Dörnbrack, A.: In-situ observations of young contrails – overview
1095   and selected results from the CONCERT campaign, Atmos. Chem. Phys., 10, 9039–9056, doi:10.5194/acp-10-9039-2010,
1096   2010.

1097

1098   Voigt, C., Jeßberger, P., Jurkat, T., Kaufmann, S., Baumann, R., Schlager, H., Bobrowski, N., Guffirda, G., and Salerno, G.:
1099   Evolution of CO_2, SO_2, HCl and HNO_3 in the volcanic plumes from Etna, Geophys. Res. Lett., 41,
1100   doi:10.1002/2013GL058974, 2014.

1101

1102   Voigt, C., Schumann, U., Minikin, A., Abdelmonem, A., Afchine, A., Borrmann, S., Boettcher, M., Buchholz, B., Bugliaro,
1103   L., Costa, A., Curtius, J., Dollner, M., Dörnbrack, A., Dreiling, V., Ebert, V., Ehrlich, A., Fix, A., Forster, L., Frank, F.,
1104   Fütterer, D., Giez, A., Graf, K., Grooß, J., Groß, S., Heimerl, K., Heinold, B., Hüneke, T., Järvinen, E., Jurkat, T., Kaufmann,
1105   S., Kenntner, M., Klingebiel, M., Klimach, T., Kohl, R., Krämer, M., Krisna, T. C., Luebke, A., Mayer, B., Mertes, S.,
1106   Molleker, S., Petzold, A., Pfeilsticker, K., Port, M., Rapp, M., Reutter, P., Rolf, C., Rose, D., Sauer, D., Schäfler, A., Schlage,

R., Schnaiter, M., Schneider, J., Spelten, N., Spichtinger, P., Stock, P., Walser, A., Weigel, R., Weinzierl, B., Wendisch, M., Werner, F., Wernli, H., Wirth, M., Zahn, A., Ziereis, H., and Zöger, M.; ML-CIRRUS: The Airborne Experiment on Natural Cirrus and Contrail Cirrus with the High-Altitude Long-Range Research Aircraft HALO, B. Am. Meteorol. Soc. 98(2), 271-288, doi:bams-d-15-00213.1, 2017.

Voigt, C., Lelieveld, J. , Schlager, H., Schneider, J., Sauer, D., Meerkötter, R., Pöhlker, M., Bugliaro, L., Curtius, J., Erbertseder, T., Hahn, V., Jöckel, P., Li, Q., Marsing, A., Mertens, M., Pöhlker, C., Pöschl, U., Pozzer, A., Tomsche, L., and Schumann, U.: Aerosol and Cloud Changes during the Corona Lockdown in 2020 - First highlights from the BLUESKY campaign; EGU21-13134, https://meetingorganizer.copernicus.org/EGU21/session/40818, 2021.

Wang, M., Zhao, K., Pan, Y., Xue, M.: Evaluation of simulated drop size distributions and microphysical processes using polarimetric radar observations for landfalling Typhoon Matmo (2014), J. Geophys. Res. Atmos., 125, 1-20, doi:10.1029/2019JD031527, 2020.

Weissmann, M., M. Göber, C. Hohenegger, T. Janjic, J. Keller, C. Ohlwein, A. Seifert, S. Trömel, T. Ulbrich, K. Wapler, C. Bollmeyer, H. Deneke: The Hans-Ertel Centre for Weather Research – Research objectives and highlights from its first three years. Meteorol. Z., 23(3), 193 – 208, 2014.

Wendisch, M., Pöschl, U., Andreae, M. O., Machado, L. A. T., Albrecht, R., Schlager, H., Rosenfeld, D., Martin, S. T., Abdelmonem, A., Afchine, A., Araùjo, A. C., Artaxo, P., Aufmhoff, H., Barbosa, H. M. J., Borrmann, S., Braga, R., Buchholz, B., Cecchini, M. A., Costa, A., Curtius, J., Dollner, M., Dorf, M., Dreiling, V., Ebert, V., Ehrlich, A., Ewald, F., Fisch, G., Fix, A., Frank, F., Fütterer, D., Heckl, C., Heidelberg, F., Hüneke, T., Jäkel, E., Järvinen, E., Jurkat, T., Kanter, S., Kästner, U., Kenntner, M., Kesselmeier, J., Klimach, T., Knecht, M., Kohl, R., Kölling, T., Krämer, M., Krüger, M., Krisna, T. C., Lavric, J. V., Longo, K., Mahnke, C., Manzi, A. O., Mayer, B., Mertes, S., Minikin, A., Molleker, S., Münch, S., Nillius, B., Pfeilsticker, K., Pöhlker, C., Roiger, A., Rose, D., Rosenow, D., Sauer, D., Schnaiter, M., Schneider, J., Schulz, C., de Souza, R. A. F., Spanu, A., Stock, P., Vila, D., Voigt, C., Walser, A., Walter, D., Weigel, R., Weinzierl, B., Werner, F., Yamasoe, M. A., Ziereis, H., Zinner, T., and Zöger, M.: ACRIDICON–CHUVA Campaign: Studying Tropical Deep Convective Clouds and Precipitation over Amazonia Using the New German Research Aircraft HALO, B. Am. Meteorol. Soc., 97(10), 1885-1908, doi:bams-d-14-00255.1, 2016.

Wolfensberger, D. and Berne, A.: From model to radar variables: a new forward polarimetric radar operator for COSMO, Atmos. Meas. Tech., 11, 3883-3916, doi: 10.5194/amt-11-3883-2018, 2018.

Xie, X., Evaristo, R., Trömel, S., Saavedra, P., Simmer, C., and Ryzhkov, A.: Radar Observation of Evaporation and Implications for Quantitative Precipitation and Cooling Rate Estimation, J. Atmos. Oceanic Technol. 33(8), 1779-1792, doi:10.1175/JTECH-D-15-0244.1, 2016.

1137

Xie, X., Shrestha, P., Mendrok, J., Carlin, J., Trömel, S., and Blahak, U.: Bonn Polarimetric Radar forward Operator (B-PRO), CRC/TR32 Database (TR32DB), doi:10.5880/TR32DB.41, 2021, (accessed 8 April 2021).

Xue, L., Fan, J., Lebo, Z. J., Wu, W., Morrison, H., Grabowski, W. W., Chu, X., Geresdi, I., North, K., Stenz, R., Gao, Y., Lou, X., Bansemer, A., Heymsfield, A. J., McFarquhar, G. M., and Rasmussen, R. M.: Idealized Simulations of a Squall Line from the MC3E Field Campaign Applying Three Bin Microphysics Schemes: Dynamic and Thermodynamic Structure, Monthly Weather Review, 145(12), 4789-4812, doi:10.1175/MWR-D-16-0385.1, 2017.

You, C.-R., Chung, K.-S., and Tsai, C.-C.: Evaluating the performance of convection-permitting model by using dual-polarimetric radar parameters: Case study of SoWMEX IOP8, Remote Sensing, 12(18):3004, 1-25, doi:10.3390/rs12183004, 2020.

Zängl, G., et al.: The ICON (icosahedral non-hydrostatic) modelling framework of DWD and MPI-M: Description of the non-hydrostatic dynamical core, Q. J. Roy. Meteor. Soc., 141, 563–579, 2015.

Zeng, Y., Janjic, T., Lozar, A. de, Welzbacher, C. A., Blahak, U., and Seifert, A.: Assimilating radar radial wind and reflectivity data in an idealized setup of the COSMO-KENDA system, Atmospheric Research, 249, 105282, doi:10.1016/j.atmosres.2020.105282, 2021a.

Zeng, Y., Janjic, T., Feng, Y., Blahak, U., de Lozar, A., Bauernschubert, E., Stephan, K., and Min, J.: Interpreting estimated observation error statistics of weather radar measurements using the ICON-LAM-KENDA system, Atmos. Meas. Tech., 14, 5735–5756, https://doi.org/10.5194/amt-14-5735-2021, 2021b.

Zeng, Y., Janjic, T., Lozar, A. de, Rasp, S., Blahak, U., Seifert, A., and Craig, G. C.: Comparison of methods accounting for subgrid-scale model error in convective-scale data assimilation, Mon. Wea. Rev., 148, 2457-2477, 2020.

Zeng Y., Janjic, T., Sommer, M., Lozar, A. de, Blahak, U., and Seifert, A.: Representation of model error in convective-scale data assimilation: additive noise based on model truncation error, J. Adv. Model. Earth Sy., 11, 752-770, 2019.

Zeng. Y., Janjic, T., Lozar, A. de, Blahak, U., Reich, H., Keil, C., and Seifert, A.: Representation of model error in convective-scale data assimilation: Additive noise, relaxation methods and combinations, J. Adv. Model. Earth Sy., 10, 2889–2911, 2018.

1169

1170   Zeng, Y., Blahak, U., and Jerger, D.: An efficient modular volume-scanning radar forward operator for NWP models:

1171   description and coupling to the COSMO model, Q. J. Roy. Meteor. Soc., 142(701), 3234-3256, 2016

1172

1173   Zhu, K., Xue, M., Ouyang, K., and Jung, Y.: Assimilating polarimetric radar data with an ensemble Kalman filter: OSSEs with

1174   a tornadic supercell storm simulated with a two-moment microphysics scheme, Q. J. Roy. Meteor. Soc., 146: 1880– 1900,

1175   doi:10.1002/qj.3772, 2020.

1176

1177
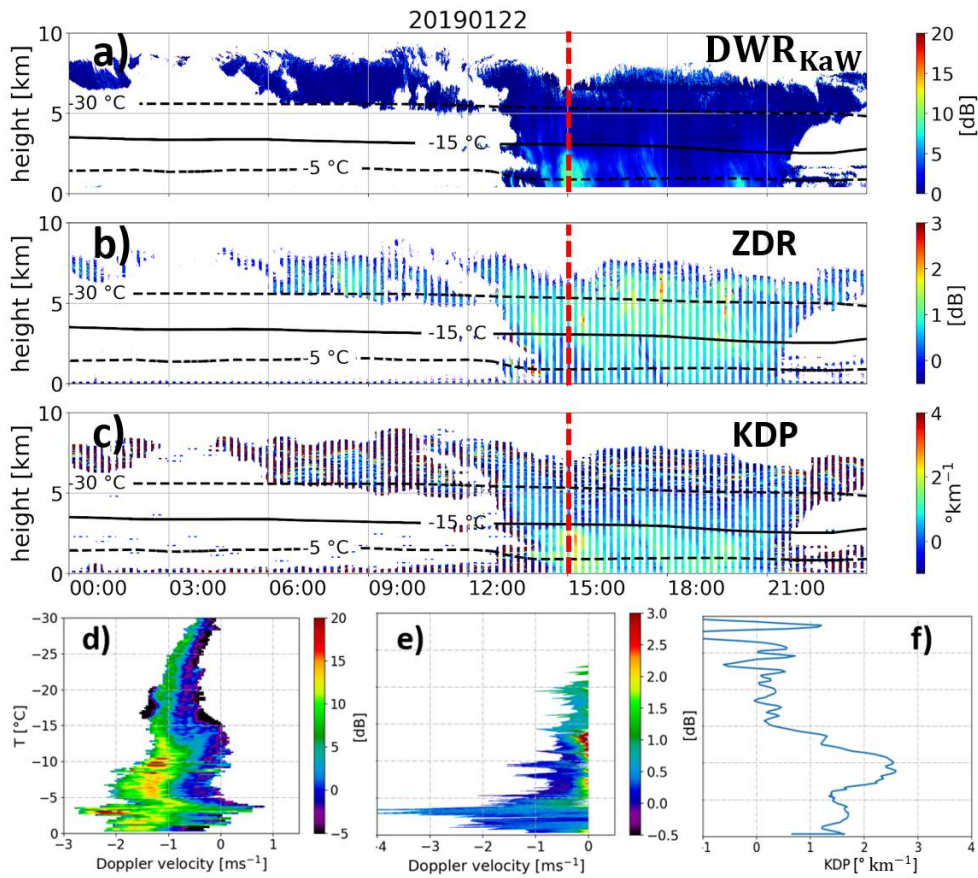
1179   **Figure 1: Observations at JOYCE-CF shows a) DWRKaW, b) Z$_{DR}$ (measured at a 30° elevation angle), c) K$_{DP}$ (also measured at 30°**

1180   **elevation angle) on 22 January 2019. Panels d)-f) show the observed DWR-spectrum, Z$_{DR}$-spectrum and K$_{DP}$-profile at 15:00 UTC**

1181   **(indicated by the red line in panels a)-c))**

1182

1183

1184

1185
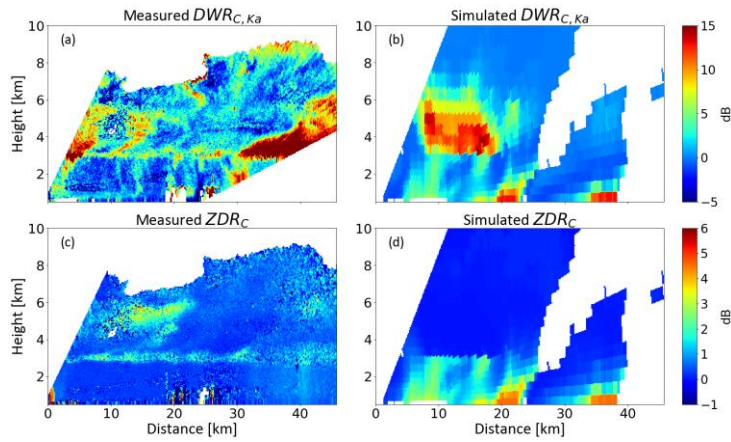
Figure 2 (a) Dual-wavelength ratio between the C-band POLDIRAD and Ka-band miraMACS measurements on the 7th July 2019,
(b) simulated dual-wavelength ratio, (c) differential radar reflectivity Z$_{DR}$ measured by the C-band radar POLDIRAD, and (d)
simulated Z$_{DR}$ of a comparable, but not identical, precipitation event using the P3 scheme (Morrison and Milbrandt, 2015).
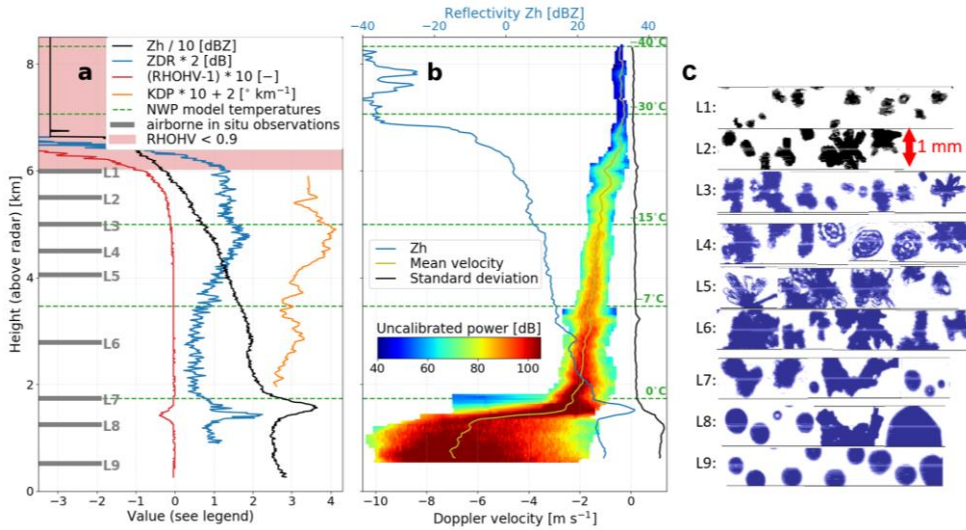
Figure 3: Measurements of slant-viewing and zenith-pointing polarimetric C-band weather radar scans with NWP model based temperature levels and airborne in-situ observations: (a) quasi-vertical profiles (QVPs) of radar reflectivity Z_H, differential reflectivity Z_{DR}, copolar cross-channel correlation coefficient ρ_{HV}, and the specific differential phase K_{DP} estimated from (noisy) measurements of the differential phase by aggressive filtering above the melting layer; (b) average Doppler spectra from a 15 s birdbath scan and corresponding first 3 moments at each radar bin height: reflectivity, power-weighted mean velocity and standard deviation; (c) in situ particle images (downward-looking projection images) collected at altitudes L1 to L9.
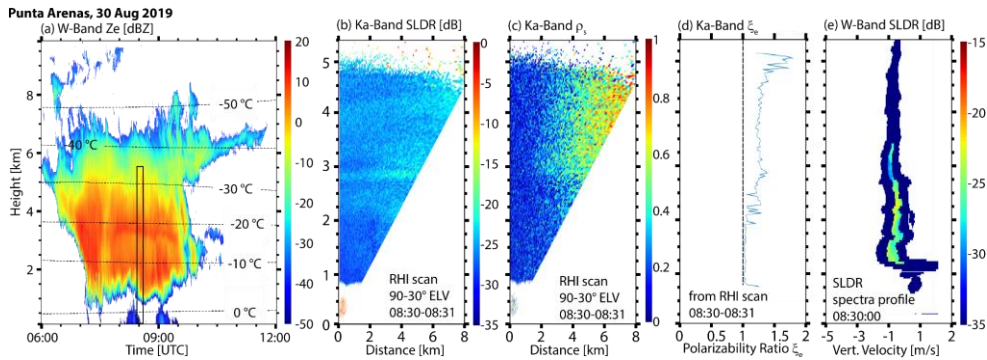
Figure 4: Case study of a deep mixed-phase cloud event observed with multiwavelength polarimetric cloud radars at Punta Arenas, Chile, on 30 August 2019. (a) vertical-pointing W-Band (94-GHz) radar reflectivity factor Ze and isolines of modeled air temperature, (b) and (c) Ka-Band (35-GHz) RHI scans (90°-30° elevation) of slanted linear depolarization ratio SLDR and co-cross correlation coefficient in the slanted basis ρ_s, respectively, from 08:30-08:31 UTC, (d) profile of the shape index polarizability ratio (ξ_e) obtained from the RHI scans shown in (b) and (c), and (e) height spectrogram (at 90° elevation) of W-Band SLDR from 08:30:00 UTC. The time and height frame of panels (b-e) is indicated by the black rectangle in (a).

1208
1209
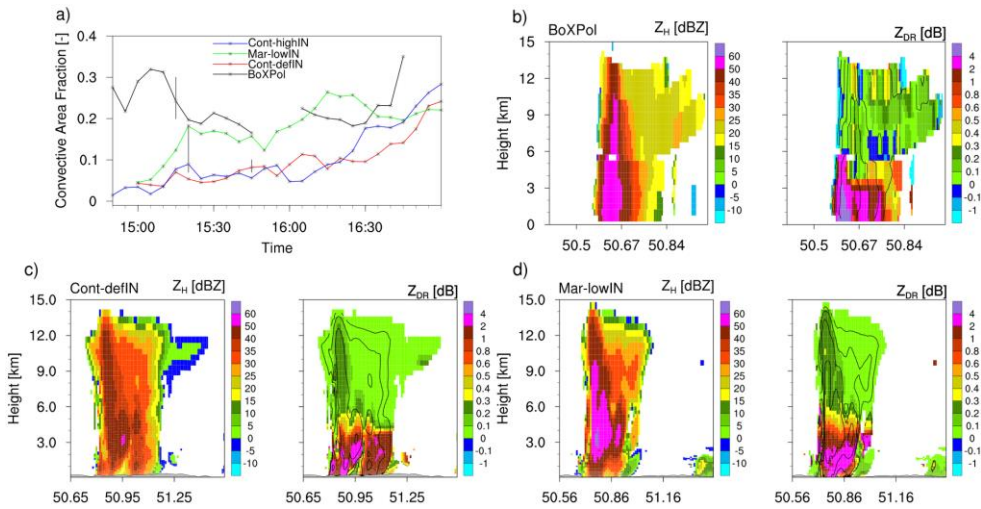
1210 **Figure 5: Time-series of Convective Area Fraction (CAF) evolution (panel a) and reconstructed observed (panel b) and**
1211 **simulated/synthetic range-height-indicators (RHI) of horizontal reflectivity Z_H and differential reflectivity Z_{DR} (panels c and d).**
1212 **Synthetic RHIs are based on simulations for actual land-cover with different perturbations of CN and IN concentrations, where**
1213 **Cont-defIN indicates continental aerosol with default IN concentration and Mar-lowIN indicates maritime aerosol with low IN**
1214 **concentration. The gaps in the BoXPol-observed CAF time series are due to strong attenuation. The vertical grey bars (panel a)**
1215 **indicate the times at which the RHIs are compared.**

1216

1217
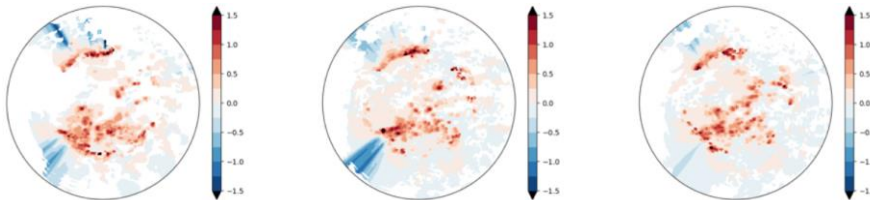
1218 **Figure 6: Synthetic PPI of Z_{DR} at 0.5 deg elevation for the DWD radar site Neuheilenbach based on the analysis obtained for June**
1219 **4 at 16:00 UTC by assimilation of radar reflectivity and using three different ways to specify the model error: large scale uncertainty**
1220 **(left), large plus unresolved scales uncertainty (middle) and in addition the use of the warm bubble approach (right).**
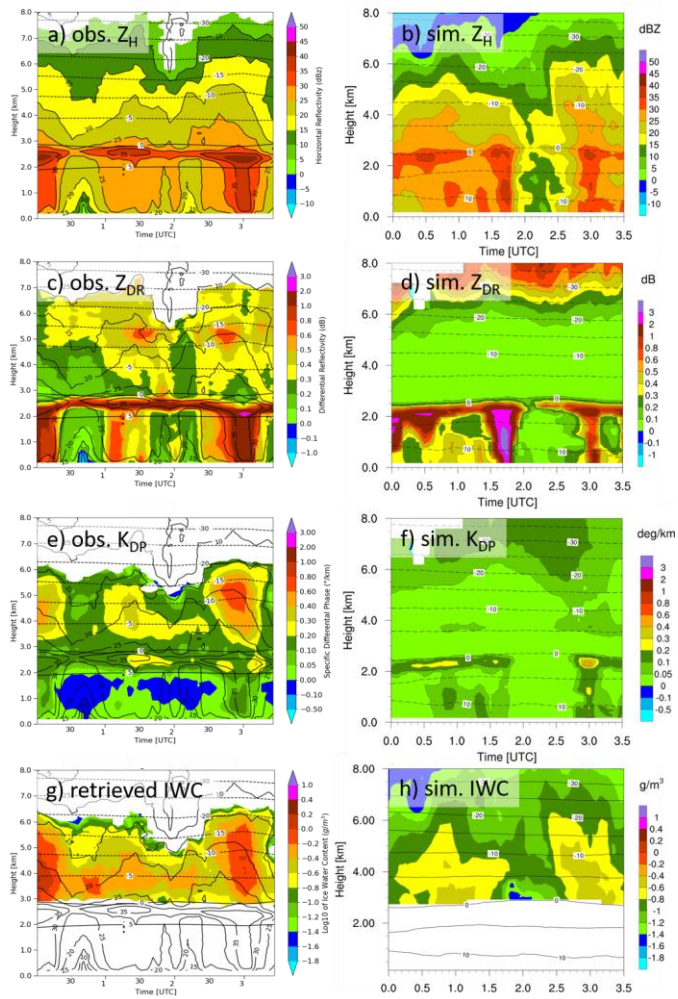
1221

Figure 7: Quasi-vertical profiles (QVPs) of observed (left column) and simulated (right column) polarimetric radar variables horizontal reflectivity Z_H (panels a and b), differential reflectivity Z_DR (panels c and d), specific differential phase K_DP (panels e and f), together with radar-retrieved (panel g) and simulated ice water content (IWC, panel h). The QVPs show a stratiform rain event

1225   **observed on 7 October 2014 between 0:00 and 3:30 UTC with the polarimetric X-band radar in Bonn, BoXPol, and simulated with**

1226   **COSMO version 5.1 and the 2-moment cloud microphysics scheme.**

1227
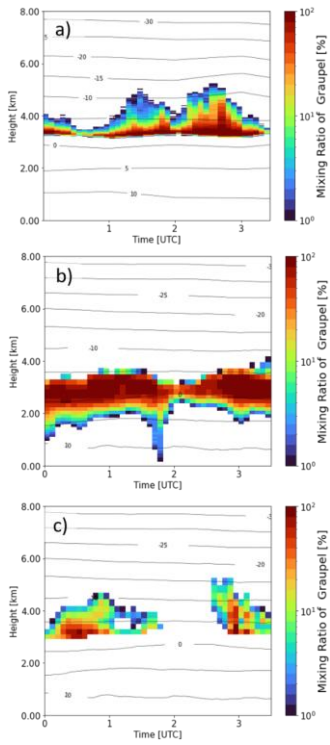
1228

1229   **Figure 8: Retrieved and simulated graupel mixing ratios, defined as the percentage of graupel in the total hydrometeor mass, for**

1230   **the stratiform rain event shown in Fig. 7 (7 October 2014, 0:00-3:30 UTC). An advanced hydrometeor classification and**

1231   **quantification algorithm has been applied to polarimetric BoXPol measurement (panel a) and to simulated radar variables based**

1232   **on COSMO simulations (panel c) and compared to the COSMO-simulated graupel mixing (panel b).**

1233

1234

1235

1236
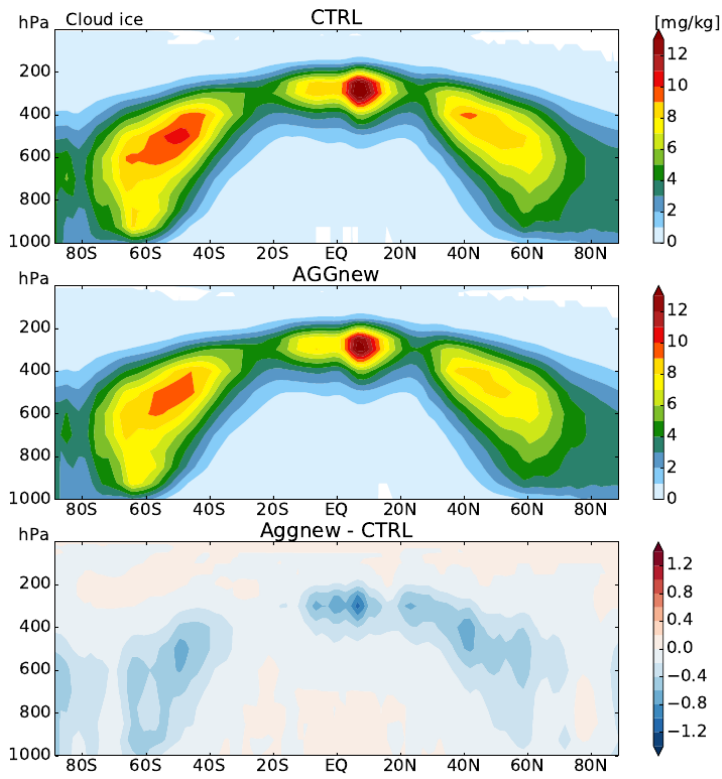
1237

Figure 9: Specific ice water, q_i, [g kg^{-1}] as zonal, annual mean for (top) standard ICON GCM output, (middle) aggregation parameterization revised as stochastic parameterization drawing from the q_i subgrid-variability PDF, and (bottom) difference between the two.

1241

1242

1243

1244

1245